공학박사 학위논문

Ruthenium-based catalysts for the conversion of marine biomass-derived chemicals

해조류 바이오매스 유래 화합물 전환을 위한 루테늄 기반 촉매계 연구

2023년 2월

서울대학교 대학원
화학생물공학부

양 승 도

Ruthenium-based catalysts for the conversion of marine biomass-derived chemicals

지도 교수 김 도 희

이 논문을 공학박사 학위논문으로 제출함

2023 년 1 월

서울대학교 대학원

화학생물공학부

양 승 도

양승도의 공학박사 학위논문을 인준함

2023 년 1 월

위 원 장	이 원 보	(인)
부위원장	김 도 희	(인)
위 원	강 종 헌	(인)
위 원	김 지 만	(인)
위 원	박 영 권	(인)

Abstract

Carbon neutral policy at the national level to limit the increase in the global average temperature to within 1.5 ℃ is no longer an option but a mandatory national policy. In line with this global trend, South Korea is also planning to implement the Carbon Neutrality Framework Act, which enacts economic and social transition to achieve carbon neutrality by 2050. In this process, maximizing the utilization of renewable energy is the most crucial task. Renewable energy refers to energy collected from renewable resources, that is, resources that are naturally replenished over time, such as sunlight, wind, tidal, biological resources (biomass), and geothermal heat. Among them, research on solar and wind energy for power generation is being intensively conducted. On the other hand, biomass is the only renewable carbon source that can replace petroleum-based refineries to produce various chemical products.

Biorefinery refers to a refinery that converts biomass to energy and chemicals such as fuels, plastics, and fibers. The features of the biorefinery can be classified into four categories: (1) platform, (2) product, (3) feedstocks, and (4) process, and each feature consists of various subgroups. There are several issues such as supply-chain of

feedstocks, greenhouse gas emissions, and competitive price for the design of a biorefinery under the classification system. In consideration of the above issues, marine biomass has advantageous features that are a non-edible resource and has rapid growth with a lignin-free structure, unlike terrestrial biomass. Among marine biomass feedstocks, alginic acid polymer, a major component of brown algae, contains carboxyl groups, inducing the production of various products that cannot be obtained from lignin or cellulose, which are representative platforms of terrestrial biomass. Especially, chemical products can be more diversified depending on the heterogeneous catalytic system used in the thermochemical conversion process of alginic acid.

In this thesis, the hydrothermal reaction of marine biomass-derived alginic acid and its intermediates as reactants was mainly conducted under a ruthenium-based catalytic system. Accordingly, a promoter to diversify the chemical portfolio from alginic acid and a strategy for the catalytic system to increase the efficiency of ruthenium was investigated.

Firstly, it was attempted to expand the chemical portfolio from alginic acid by using base promoters, which raise the pH of the aqueous solution. Hydrogenolysis of alginic acid over ruthenium and ruthenium-nickel supported on activated carbon catalysts was

performed in a batch reactor using base promoters such as NaOH, $CaCO_3$, $Ca(OH)_2$, and $Mg(OH)_2$. Among the promoters, NaOH provides the highest carbon efficiency and yield of glycols, such as ethylene glycol and propylene glycol (1,2-propanediol). In addition, various organic acids such as lactic acid, glycolic acid, and formic acid were produced in the form of salts. The hydrogenolysis of potential intermediates such as sorbitol, mannitol, xylitol, lactic acid, and glycolic acid demonstrated direct conversion of alginic acid to glycols without reaction intermediates such as sugar alcohols and organic acids. Furthermore, ruthenium-nickel bimetallic catalysts as a function of the nickel/ruthenium molar ratio were used to increase the yield and selectivity of glycols. The highest yield of glycols, 24.1%, was obtained when the nickel/ruthenium molar ratio was 1, due to the enhanced electronic interaction between ruthenium and nickel.

Research to improve the efficiency of a heterogeneous catalyst is an essential strategy for enhancing the production efficiency of highly sustainable biorefineries. Alginic acid is converted into high value-added sugar alcohols such as sorbitol and mannitol via hydrolytic hydrogenation over a ruthenium-based heterogeneous catalyst. To improve the efficiency of ruthenium in the above catalytic system, it was attempted to verify the inter-particle

hydrogen spillover mechanism in the liquid-phase hydrogenation. Ruthenium catalysts loaded on various supports such as activated carbon, SiO_2, TiO_2, and Al_2O_3 were prepared and applied in the liquid-phase hydrogenation of gluconic acid - an intermediate in the hydrolytic hydrogenation of alginic acid. When activated carbon was mixed as an additive with the oxide-supported ruthenium catalysts, the turnover rate of ruthenium in the hydrogenation of gluconic acid increased from 12.8 h^{-1} to 38.8 h^{-1}, particularly for Ru/SiO_2. According to various analyses, activated carbon can uptake more spilt-over hydrogen from ruthenium and exhibit superior adsorption ability for reactants compared to other metal oxides, thereby providing additional catalytically active sites. As a result, the simple strategy of adding pristine AC resulted in a significantly enhanced turnover rate of the oxide-supported ruthenium catalyst.

In this thesis, the conversion of marine biomass-derived alginic acid and its intermediates was performed over ruthenium-based catalytic systems. The conversion of alginic acid into glycols is significant in that it further diversified alginic acid-derived products. In addition, the improvement of the efficiency of ruthenium in the hydrogenation through the addition of pristine activated carbon highlighted the potential for a physical mixing strategy in the liquid-phase. Thus, it is expected that this thesis will draw attention to

research on biorefinery of marine biomass and enable more efficient utilization of active metals.

Keyword : Alginic acid; gluconic acid; hydrogenolysis; hydrogenation; glycol; sorbitol; ruthenium catalyst; activated carbon

Student Number : 2017-20748

Contents

List of Schemes

List of Figures

List of Tables

Chapter 1. Introduction

1.1. The need for sustainable energy resources

One of the most important challenges over the last decades is to formulate a strategy to respond to various factors such as environmental pollution and price volatility of crude oil in the current petroleum-based society. Various environmental regulations newly established to respond to the global climate crisis act as a compulsory and compelling driving force to shift from the petroleum-based society into a sustainable society. Especially, a carbon neutral policy triggered to curb the rise in global temperature forces countries or companies to reduce their net carbon emissions and eventually to zero. For example, in the case of the European Union, it was announced the 'Fit for 55' package, a legislative package to reduce net greenhouse gas emissions by 55% compared with 1990 levels by 2030 as a policy to achieve the goal of climate neutrality by 2050[1]. Therefore, it is important to search for alternative renewable energy sources to meet the increasing energy demand and regulations.

Figure 1.1 Net renewable capacity additions, World, 2011 to 2022.

Source: Renewable Energy Market Update 2021.

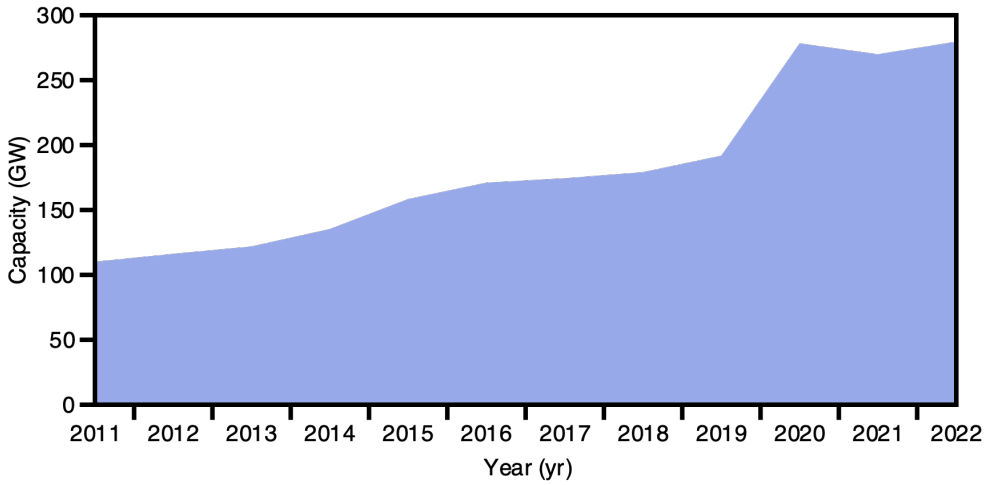

Figure 1.2 Classification of biorefinery systems.

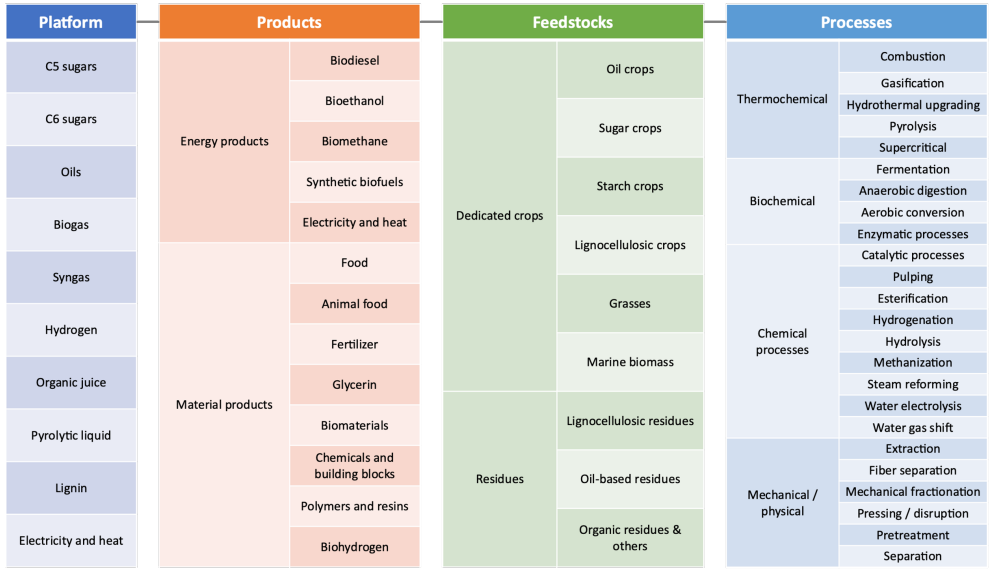

Renewable energy comprises plenty of naturally occurring resources that are constantly replenished. Alternative renewable energy sources include sunlight, water, wind, hydrogen, and biomass, which stored in the Earth. Renewable electricity obtained from such resources can be used for the transportation, residential and commercial utilization. As shown in Figure 1.1, from 2011 to 2021, additions to renewable energy capacity have grown from 110.1 GW to 269.9 GW, which is a 145% increase[2]. The systems using renewable energy include a variety of technologies. Some technologies are already mature and economically competitive, while others require further development.

1.2. Biomass as a feedstock for biorefinery

As mentioned above, although solar and wind resources are promising natural resources to generate renewable electricity, biomass resources are attractive as a sustainable carbon resource to produce important chemicals that support human life. Biomass is all organic materials that stem from plants or animals such as corn stover, wood, and algae, which can be used as a feedstock for a biorefinery. The biorefinery converts into electricity, heat, and other

beneficial chemicals. As demonstrated in Figure 1.2, biorefineries can be classified based in four main features, and each feature consists of several subgroups: (1) Platforms; (2) Products; (3) Feedstocks; (4) Processes[3]. Among features, products can be categorized in two main subgroups according to the conversion of biomass in an energetic or material product. First, energy-driven biorefinery systems produce a secondary energy carrier as biofuels, electricity, and heat. Secondly, material-driven biorefinery systems convert biomass resources into biobased products such as chemicals and building blocks. The biorefineries involves the subsequent conversion into a larger number of products. Such approach has successfully been used in petroleum-based refineries.

Most of platform chemicals to produce various other value-added products are still carbon-based resources. Given that carbon dioxide produced by industrial activities is one of the most significant contributors to the rise in global temperature, biomass can be an intriguing source to produce the chemicals. The size of biorefinery market has been continuously increasing and rapid growth is expected at a compound annual growth rate of about 11% with the rise of the carbon neutral policy[4].

A biorefinery integrates biomass conversion processes and equipment to produce fuels, energy, and chemicals. Such biorefinery

can take advantages from the design to maximize the mass and energy efficiency and minimize the waste streams[5]. For the design, there are several issues to consider: (1) supply chain of biomass; (2) greenhouse gas emissions; (3) competitive price. Even though industrialized biorefinery can solve most of the issues above, some remained unsolved. For instance, corn, agricultural crop residues, is a feedstock for biorefinery that has already been industrialized to a bioethanol, but its supply chain can be unstable because it is an edible resource[5]. In addition, such biomass causes huge greenhouse gas emissions during cultivation. Wood, forestry residues, concerns about deforestation and requires an expensive pretreatment to separate the recalcitrant lignin polymer[6]. Indeed, terrestrial-based biorefinery currently seems to be unsustainable because of environmental as well as economic impacts. Meanwhile, macroalgae, so-called marine biomass, is promising because it does not have the disadvantages of previous generations.

Scheme 1.1 Structural difference between cellulose in terrestrial biomass and alginic acid in marine biomass.

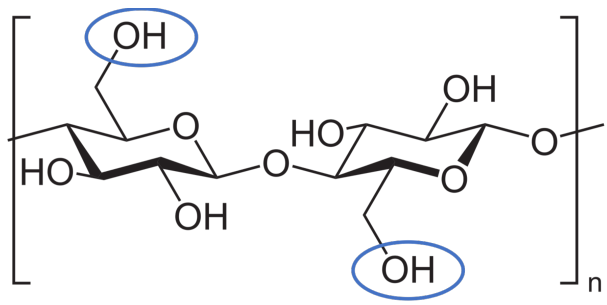

Cellulose

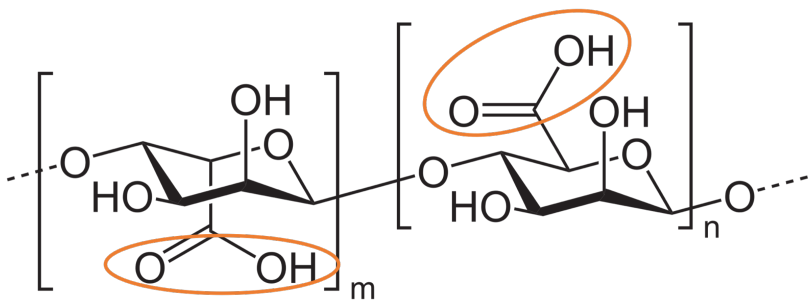

Alginic acid

Macroalgae have rarely at risk of competing for food and energy than other biomass feedstocks like corn and wheat. In addition, they do not need land and freshwater for their cultivation[6]. Although macroalgae have various environmental and economic advantages, thorough research about macroalgae-based biorefinery is essential because macroalgae have unique carbohydrates that are distinctly different from terrestrial biomass. As shown in Scheme 1.1, cellulose and alginic acid, which are representative polymers of terrestrial biomass and marine biomass resources, have the same bond but have different functional groups, which will be discussed in more detail later.

1.3. Potentials of macroalgae as a feedstock

Macroalgae, so-called seaweeds, are a class of marine biomass that live in the sea. It is divided into green algae, brown algae, and red algae according to the pigment contained therein. It is present in large quantities in the ocean and affects the surrounding creatures as nutrients, protection from waves, hiding places, and adhesion substrates. In addition, it is abundant in shallow seas and is easy to collect.

Table 1.1 World production of macroalgae biomass.[a]

Species	Group	Production (%)
Laminaria japonica	Brown algae	32.61
Eucheuma spp.	Red algae	22.11
Kappaphycus alvarezii	Red algae	11.88
Undaria pinnatifida	Brown algae	9.74
Gracilaria verrucose	Red algae	7.30
Porphyra spp.	Red algae	6.79
Gracilaria spp.	Red algae	3.58
Porphyra tenera	Red algae	3.57
Eucheuma denticulatum	Red algae	1.64
Sargassum fusiforme	Brown algae	0.50
Phaeophyceae	Brown algae	0.14
Euteromorpha clathrate	Green algae	0.07
Monostroma nitidum	Green algae	0.03
Caulerpa spp.	Green algae	0.03
Codium fragile	Green algae	0.01
Gelidium amansii	Red algae	0.01

[a] Adjusted from [7].

Table 1.2 Carbohydrate composition of brown algae (in wt%).[a]

Species	Protein	Lipid	Carbohydrates	Ash
Laminaria japonica	16.1	2.4	39.3	19.6
Undaria pinnatifida	15.0	3.2	38.0	30.8

[a] adjusted from [8].

Table 1.1 shows promising macroalgae species for biorefinery feedstock at present. Only two species of brown algae, *Laminaria Japonic* and *Undaria Pinnatifida*, account for more than 40% of the total. On the other hand, the production of green algae is insignificant. Considering the current mass-cultivation technology and market demand, macroalgae-based biorefinery needs to focus on the utilization of brown algae and red algae. Brown algae mainly consists of protein, lipid, carbohydrate, and ash, and the approximate content is shown in Table 1.2. Among them, carbohydrates are largely divided into carbohydrates and fiber, and carbohydrates are composed of alginic acid and mannitol. Alginic acid, a major polysaccharide of brown algae, accounts for up to 40% dry wt. as a principal material of the cell wall[9].

Alginic acid is known to have useful physiological activities in the body. It has been reported that it inhibits the growth of harmful microorganisms present in the intestine, lowers blood cholesterol, and controls blood sugar. Although alginic acid is a promising renewable energy source that can replace petroleum-based refineries, it is only used in limited fields such as the pharmaceutical industry and food additives. However, the replacement of crude oil infrastructure for sustainable fuel and chemical production is no longer an option as being entered into a carbon neutral society.

Therefore, in a situation where biomass is the only raw material that can generate chemicals including basic elements of carbon, oxygen, and hydrogen, research on the conversion process of alginic acid is essential.

Scheme 1.2 Structure of alginic acid and its monomers.

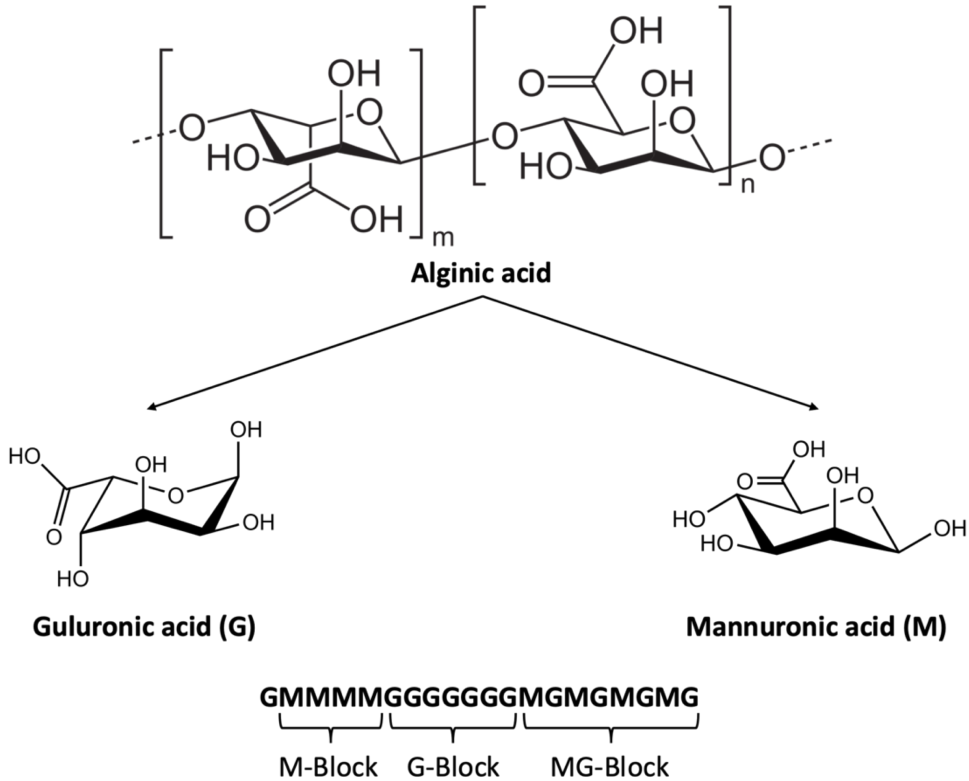

Scheme 1.3 Catalytic conversion of alginic acid into value-added platform chemicals.

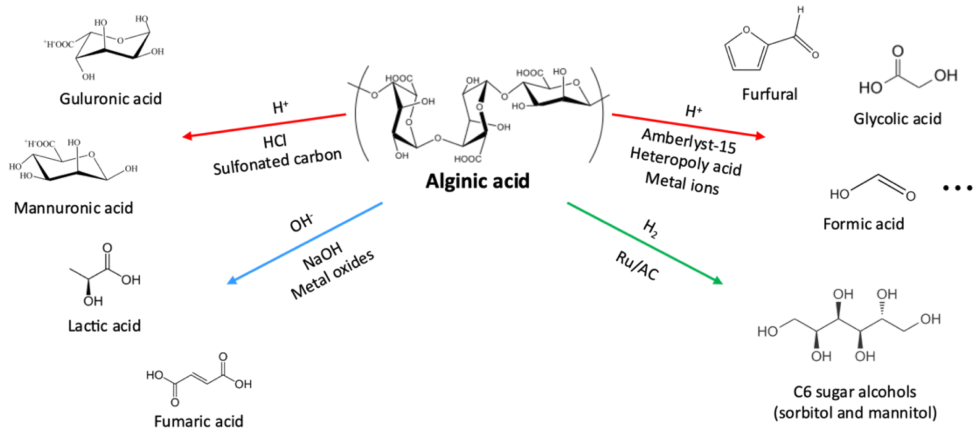

1.4. Catalytic conversion of alginic acid into platform chemicals

Currently, the production of renewable value-added chemicals in a biorefinery is highly dependent on lignocellulosic biomass feedstocks. For instance, sorbitol, which is used as a precursor of plastic monomer and raw material of vitamin C, etc., can be obtained via the hydrogenation of cellulose-derived glucose using a porous nickel catalyst. In addition, furfural, which is used as a precursor of biofuel, is made through hydrolysis and dehydration reaction of xylan and xylose derived from hemicellulose using an acid catalyst such as zeolites, metal oxides, resins, and carbon-based materials. However, since cellulose or starch, which is lignocellulosic biomass, is composed of a single glucose monomer, the types of compounds produced from the biomass are limited. In addition, the recalcitrant structure of lignin or crystalline structure of cellulose require relatively harsh reaction conditions at high temperature and pressure for a long time for thermochemical conversion. Therefore, alginic acid derived from brown algae, which is inedible, lignin-free, and has rapid growth, has significant advantages as a feedstock in a biorefinery.

As shown in Scheme 1.2, alginic acid is composed of two monomeric units, mannuronic acid (M) and guluronic acid (G), via β-1,4-glycosidic linkage which form poly M-block, poly G-block, and MG-block chains[10]. The ratio of M/G in alginic acid polymer varies with the season, location, and species. Recently, alginic acid has found new applications in the material-driven biorefinery to produce platform chemicals and value-added building blocks as well as traditional applications in the food, medical, and pharmaceutical industries. Scheme 1.3 demonstrates that valuable chemicals can be produced from alginic acid via catalytic hydrothermal reaction[11-18]. Briefly, various heterogeneous catalysts such as sulfonated carbons, heteropoly acids, and ruthenium-based activated carbon converted alginic acid into organic acids, furans, and sugar alcohols.

1.5. Objectives

Research on the conversion into valuable chemicals from biomass as the only renewable carbon source is an inevitable task accompanied by an increase in the amount of carbon emissions over the last decades. This thesis intends to add a new platform, process, or product that can be applied soon by performing biomass

conversion based on the classification system of the biorefinery (Figure 1.2).

(1) Feedstock: In contrast to a wide range of research on terrestrial biomass, there still is a paucity of studies on marine biomass. The various advantages of marine biomass have the potential to overcome the inherent disadvantages of lignocellulosic biomass, so it can be a superior alternative in biorefinery composed of lignocellulosic biomass. Alginic acid, a major component of brown algae that accounts for a large proportion of marine biomass, was selected as a feedstock because of its structural characteristics of having a carboxyl group that can diversify products more.

(2) Platforms: C6 sugars such as mannose and glucose can be obtained from monomers, mannuronic acid (M) and guluronic acid (G), via the hydrolytic hydrogenation of alginic acid. This thesis was performed to improve the one-pot catalytic conversion from alginic acid to value-added products through C6 sugars as a platform.

(3) Products: C6 sugar alcohols and shorter chain polyols are highly value-added products that can be produced from C6 sugars. This thesis intended to perform the conversion from alginic acid to polyols below C3, which has not been previously reported. In addition, the improvement of the system for the conversion of alginic acid into C6 sugar alcohols was conducted.

(4) Process: A chemical process was used to obtain alcohols from alginic acid. Hydrogenation and hydrogenolysis over a heterogeneous catalytic system based on metallic ruthenium (Ru) were utilized for the conversion into target products.

In this respect, the first objective of this thesis is to diversify the chemical portfolio from alginic acid using Ru-based activated carbon. The second is to improve the catalytic efficiency in the hydrogenation of alginic acid-derived chemical under an optimized Ru-based catalytic system. The Ru-based catalytic system was applied by loading Ru on various supports through the wet impregnation method or by the physical mixing method. Various analytical techniques were applied to elucidate a reaction pathway to form the polyols below C3 and other valuable chemicals and demonstrate a reaction mechanism about the enhanced catalytic system.

Chapter 2. Hydrogenolysis of alginic acid over Ru and bimetallic Ru/Ni-based activated carbon catalysts at high pH solution

2.1. Introduction

A biorefinery, in which renewable resources are utilized on a large scale, is a potential alternative based on biomass feedstocks[3-6, 19, 20]. Algal biomass, also known as the third-generation biomass, is inedible, lignin-free, and shows rapid growth, and has significant advantages in a biorefinery[6, 8-10]. As the main component of macroalgae, alginic acid is a good carbon source to produce various value-added chemicals such as acids and alcohols. Alginic acid is a polyuronide consisting of two types of hexuronic acid, D-mannuronic acid (M) and L-guluronic acid (G), connected by β-1,4-glycosidic bonds. The two units combine randomly to create polymer rings carrying carboxyl (-COOH), ether (-COC-), and hydroxyl (-OH) functional groups, which enable the prediction of reaction pathways and the design of value-added chemicals

converted from alginic acid. Based on such prediction, the hydrothermal decomposition of alginic acid was conducted under various conditions. Especially, Ban et al.[16-18] investigated the formation of C_6 sugar alcohols such as sorbitol and mannitol via hydrogenation of alginic acid. However, to the best of my knowledge, the hydrogenolysis of alginic acid to produce shorter chain polyols than C_6 sugar alcohols has yet to be reported. C_2 and C_3 glycols such as ethylene glycol (EG) and 1,2-propanediol (PG) can be used as surfactants, antifreeze compounds, and monomers in the synthesis of polyester fibers, and as chemicals in the pharmaceutical industry. Therefore, it is expected that the efficient conversion of alginic acid into glycols provides a platform to further improve the utilization of alginic acid as a biomass feedstock.

Meanwhile, the reaction mechanisms underlying the hydrogenolysis of biomass-derived feedstocks including cellulose, sugar alcohols and glycerol into glycols have been investigated[19, 21-25]. Since the hydrogenolysis reaction occurs via multiple steps, it is difficult to determine the precise reaction pathway under various reaction conditions. Nonetheless, several mechanisms of hydrogenolysis have been proposed based on experimental results. Montassier et al.[26] suggested that sugar alcohol forms an intermediate with unsaturated bonds via dehydrogenation and

undergoes a C-C bond cleavage via a retro-aldol reaction or a C-O bond cleavage by dehydration under basic conditions. In addition, other mechanisms have been proposed, including decarbonylation to explain the terminal C-C cleavage and the retro-Claisen reaction and the retro-Michael reaction based on by-product analysis. The authors reported that both a basic promoter and a metal catalyst play a role in the hydrogenolysis.

Based on these reaction pathways, several research groups performed hydrogenolysis using metal catalysts along with basic promoters[22, 23, 25]. Ru-based catalysts have been the most frequently used. For instance, Leo et al.[22] reported that the yield of glycols (the sum of EG and PG) from sorbitol increased significantly over Ru supported on alumina with $Ca(OH)_2$ as a base additive. While the dehydrogenation/hydrogenation reactions were activated by the Ru catalyst, the C-C bond cleavage via a retro-aldol reaction was promoted by a basic promoter, especially $Ca(OH)_2$, as well as a basic support, resulting in improved carbon efficiency (E_c) and selectivity to glycols. Also, Rivière et al.[23] reported that the addition of a basic promoter shifted the hydrogenolysis reaction pathway of xylitol from fast epimerization and decarbonylation to retro-aldol reaction over Ru-based catalysts. Thus, basic promoters play a crucial role in changing the selectivity to glycols.

Ni generally enhances the activity in the hydrogenation and hydrogenolysis of biomass feedstock[22, 27-31]. According to Banu et al.[27], among Ni, Pt, and Ru supported on NaY catalysts, Ni-NaY was the most efficient catalyst in the hydrogenolysis of sorbitol to EG and PG with a selectivity of 7% and 69%, respectively. Ni has also been used as a bimetallic catalyst in combination with other noble metals. Ribeiro et al.[31] reported that Ru-Ni bimetallic catalysts supported on activated carbon showed superior activity in the hydrolytic hydrogenation of cellulose to sorbitol. The authors suggested that the close interaction between Ru and Ni facilitates the conversion of cellulose and the selectivity to sorbitol. Hence, it would be interesting to utilize the bimetallic Ru-Ni supported on activated carbon in the hydrogenolysis of alginic acid.

The main objective of this study is to establish the optimum reaction system for the conversion of alginic acid to glycols such as EG and PG over Ru-based activated carbon catalysts in a basic solution. To begin with, the characteristics of the prepared catalysts were investigated via X-ray diffraction (XRD), N_2 adsorption-desorption, and H_2-temperature-programmed reduction (H_2-TPR). The reaction parameters were optimized such as reaction time, temperature, hydrogen pressure, and base concentration in the hydrogenolysis reaction. Subsequently, various basic promoters such

as $CaCO_3$, $Ca(OH)_2$, $Mg(OH)_2$, and NaOH were introduced in the hydrogenolysis over Ru-based activated carbon catalysts under the optimized reaction conditions. Finally, Ni, which enhances the activity in the hydrogenolysis, was utilized in bimetallic Ru-Ni catalysts to determine the optimum Ni/Ru molar ratio.

2.2. Experimental sections

2.2.1. Materials and chemicals

Activated carbon as the support and alginic acid from brown algae as the reactant were purchased from Sigma-Aldrich. The metal precursors $RuCl_3 \cdot xH_2O$ (ruthenium chloride hydrate) and $Ni(NO_3)_2 \cdot 6H_2O$ (nickel nitrate hexahydrate) were purchased from Alfa-Aesar. Hexitols (HOL: sorbitol, mannitol, and galactitol), pentitols (POL: xylitol, arabitol, and adonitol), tetritols (TOL: erythritol and threitol), EG, and PG were obtained from Alfa-Aesar, and were utilized as analytical standards or reactants except for threitol (from TCI, Tokyo Chemical Industry). Organic acids (lactic acid, glycolic acid, and formic acid) and basic promoters ($CaCO_3$, $Ca(OH)_2$, $Mg(OH)_2$, and NaOH) were purchased from Sigma-Aldrich. For derivatization of liquid-product samples, N,O-bis(trimethylsilyl)trifluoroacetamide (BSTFA) was obtained from

Alfa-Aesar. All chemicals were utilized without further purification or treatment.

2.2.2. Catalyst preparation

A wet impregnation method was used for the preparation of Ru-based activated carbon catalysts. The loading amount of the metals such as Ru and Ni in monometallic activated carbons, which are denoted as Ru/AC and Ni/AC, respectively, was 5 wt%. Ru-based bimetallic catalysts were prepared as a function of the Ni/Ru molar ratio, and at this time, the loading amount of Ru was maintained at 5 wt%. The resultant bimetallic catalysts were denoted as $RuNi_x$/AC, where x stands for the molar ratio of Ni to Ru. A 150 mL solution containing metal precursors was stirred with 2 g of activated carbon for 2 h, and then evaporated using a rotary evaporator followed by drying in an oven at 105 ℃ overnight. The dried powders were reduced in a muffle furnace at 250 ℃ (Ru/AC) and 500 ℃ (Ni/AC and $RuNi_x$/AC) for 2 h under 5% H_2/N_2 stream (100 ccm), and the reduced catalysts were passivated under 3% O_2/N_2 (100 ccm) at room temperature.

2.2.3. Catalyst characterization

Inductively coupled plasma-atomic emission spectroscopy (ICP-AES) was used (SHIMADZU/ICPE-9000) to determine the content of Ru and Ni in the catalysts. The N_2 adsorption and desorption isotherms were obtained using a BELSORP-mini II (BEL Japan Inc.). The catalysts were pretreated in a vacuum at 200 ℃ for at least 4 h before N_2 physisorption analysis. The results of the analysis were utilized to calculate the surface area of the catalysts via the Brunauer-Emmett-Teller (BET) method. XRD patterns were obtained with a powder X-ray diffractometer (Smartlab, Rigaku) operated at a current of 30 mA and a voltage of 40 kV. H_2-TPR profiles were obtained using a BELCAT-II catalyst analyzer (BEL Japan Inc.). The pretreated samples were heated to 900 ℃ (10 ℃ min^{-1}) in 5% H_2/Ar flow. X-ray photoelectron spectroscopy (XPS, Thermo Scientific) of the catalysts in the region of Ru3p was performed to investigate surface chemical states of Ru with AlKα μ-focused monochromatic source (1486.6 eV) at a current of 3 mA and a voltage of 12 kV. The binding energies were calibrated by calibrating the binding energy of C 1s peaks of all catalysts at 284.5 eV.

Figure 2.1 Batch reactor system

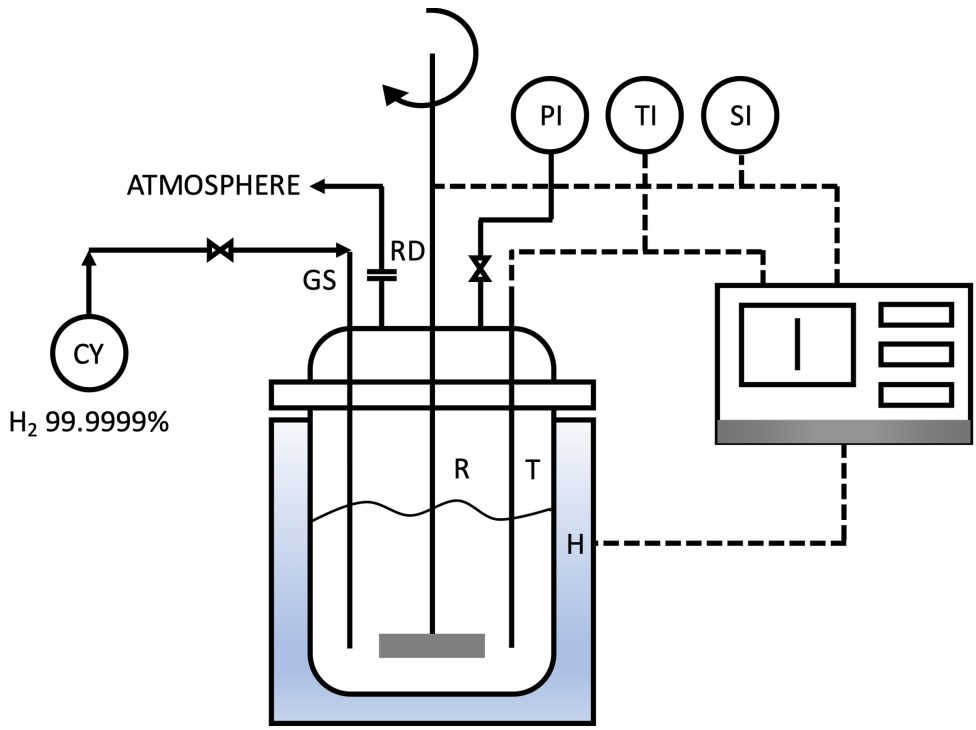

2.2.4. Catalytic activity

As shown in Figure 2.1, the hydrogenolysis of alginic acid was carried out in a 100 mL autoclave (Parr Instrument Company) after charging alginic acid or other reactants (0.3 g), deionized water including basic promoters (30 mL), and a catalyst (0.1 g). The autoclave was heated to the target temperature (8-9 ℃ min^{-1}) while stirring at 1000 rpm under high-pressure H_2 gas after purging three times with 99.999% Ar to remove the air inside. The hydrogenolysis reaction was conducted at 150-240 ℃ for 0.3-4 h under 10-70 bar. After the reaction, the reactor was rapidly quenched in an ice-cold bath and the liquid-product in the reactor was collected manually.

2.2.5. Product analysis

The molecular weight distribution of alginic acid was analyzed by a gel permeation chromatography (GPC, Thermo Dionex HPLC Ultimate3000 RI System). 0.1 M of sodium azide aqueous solution was used as a mobile phase at 40 ℃ (1 mL/min). The GPC calibration was conducted using Pullulan with a molecular weight distribution from 342 to 80,500. C_2-C_6 polyols contained in the liquid-product were quantified via gas chromatography (GC, Agilent 6890 equipped

with a DB-5 column). For the derivatization of the liquid-sample, it was pretreated via silylation with BSTFA as reported by Yang et al.[32]. High-performance liquid chromatography (HPLC using a VW detector, Agilent 1200 Series equipped with an Aminex HPX-87H column) at a column temperature of 65 ℃ and a flow rate of 0.6 mL min^{-1} in the presence of 5 mM sulfuric acid was used to quantify organic acids in the liquid-product. All the polyols and organic acids were calibrated using the external standard. By-products such as char and gas-phase products, which are not included in the liquid-products, were measured based on the difference between the total organic carbon (TOC, Sievers 5310C (GE)) of the liquid-product and the standard TOC of alginic acid. Based on the data obtained, the carbon yield was calculated as follows: $Y_{product}$ (%) = 100 × (number of carbon species in an organic compound/6) × (moles of an organic compound in the product mixture/ moles of a repeating unit in alginic acid of 0.3 g). In addition, since the conversion of alginic acid, a polymer, cannot be calculated, carbon efficiency (E_c) was used to represent the conversion efficiency of the reaction system. E_c was calculated as follows: E_c (%) = Y_{HOL} + Y_{POL} + Y_{TOL} + Y_{BDO} + Y_{PG} + Y_{EG} + Y_{LA} + Y_{GA} + Y_{FA} (HOL: sorbitol, mannitol, and galactitol; POL: xylitol, arabitol, and adonitol; TOL: erythritol and threitol; BDO: 1,2-butanediol; PG: 1,2-propanediol; EG: ethylene glycol; LA: lactic acid;

GA: glycolic acid; FA: formic acid).

Table 2.1 Surface area and atomic loading of mono and bimetallic Ru-Ni supported on activated carbon.

Catalyst	Surface area[a] ($m^2\ g^{-1}$)	Atomic loading[b] (wt%)		
		Ru	Ni	Ni/Ru[c]
AC	1033	-	-	-
Ru/AC	774	4.4	-	-
$RuNi_{0.5}$/AC	883	4.6	1.1	0.4
$RuNi_1$/AC	850	4.5	3.0	1.1
$RuNi_2$/AC	815	5.2	6.4	2.1
Ni/AC	845	-	5.9	-

[a] Calculated by the BET method.
[b] Measured by ICP-AES.
[c] Ni/Ru molar ratio.

Figure 2.2 XRD diffractograms of mono and bimetallic Ru-Ni supported AC.

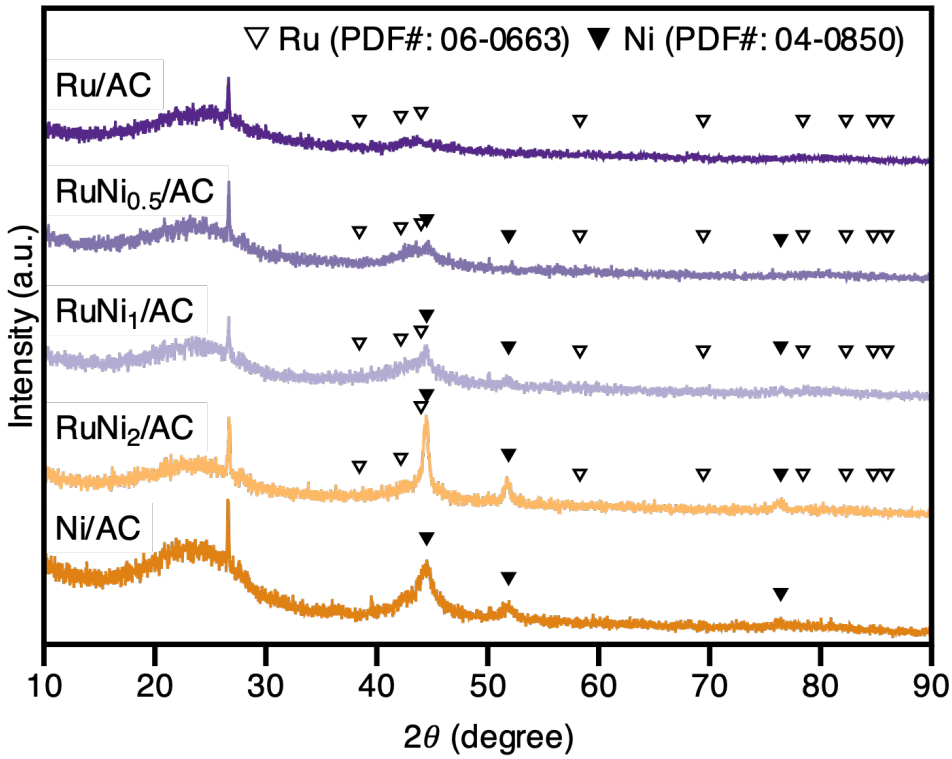

2.3. Results and discussion

2.3.1. Catalyst characterization

The surface area and atomic loading of the prepared catalysts are summarized in Table 2.1. All the metals supported on AC samples demonstrated a decrease in the BET surface area compared with the AC support, although no significant change was found in the BET surface area of the metal- containing samples as a function of the Ru/Ni molar ratio. The atomic loading of the metals in the catalyst matched strongly with the one initially designed, resulting in a reliable Ni/Ru ratio with about 10% error.

The crystallinity of Ru and/or Ni supported on activated carbon catalysts was analyzed by XRD. As shown in Figure 2.2, no X-ray diffraction peaks assigned to Ru species were detected in any sample. It is suggested that amorphous RuO_2 formed or Ru with a small crystallite size was highly dispersed during the passivation process[33]. However, diffraction peaks were detected at 2θ = 44.5° and 51.9° attributed to metallic Ni in the Ni/AC sample. In the case of bimetallic Ru/Ni catalysts, as the amount of Ni added increased, the peak of metallic Ni turned sharper without shifting the peak position, indicating the crystallization of Ni rather than the formation of Ru/Ni alloy.

Figure 2.3 H_2-TPR profiles of Ru and/or Ni supported on AC.

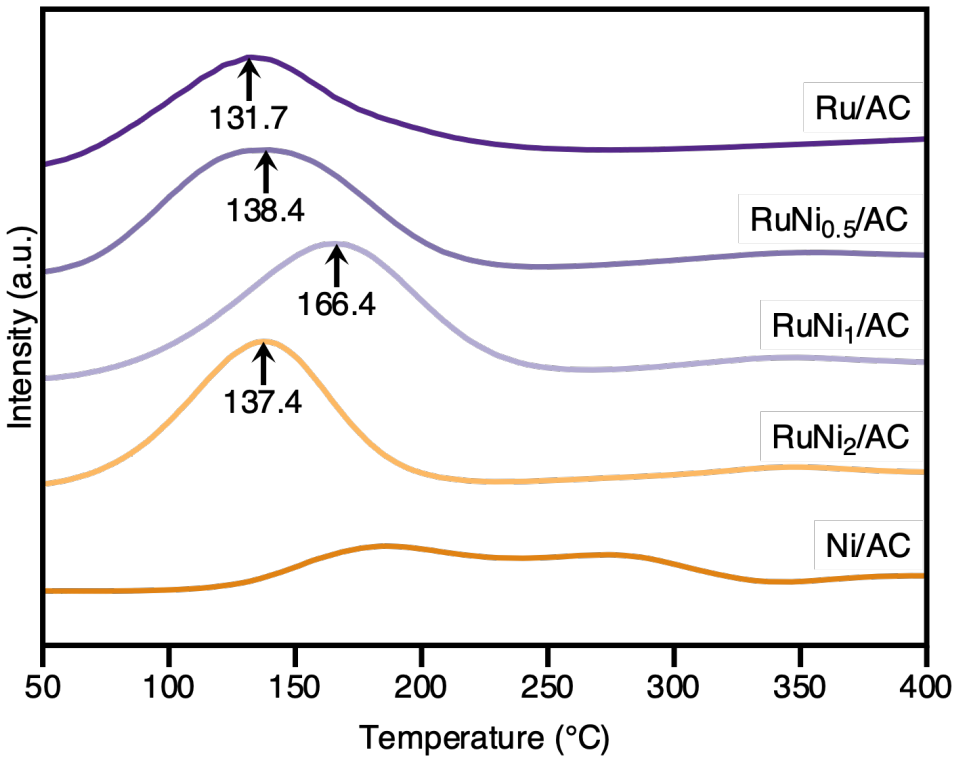

H_2-TPR was performed to elucidate the reductive property of metallic species in catalysts. As shown in Figure 2.3, Ni/AC exhibited two broad reduction peaks at *ca.* 150-350 ℃ resulting from various interactions between nickel oxide phases and surface functional groups of activated carbon [34], whereas Ru/AC exhibited a single peak of reduction due to the reduction of RuO_x to Ru at 131.7 ℃ [33]. All of the Ru/Ni bimetallic catalysts present a single peak of reduction suggesting the onset of a close interaction between Ni and Ru [35, 36]. In addition, the reduction peaks of all bimetallic catalysts were shifted to a higher temperature compared to the temperature in Ru/AC. Notably, the reduction peak of Ru/Ni species shifted to a higher temperature by ca. 34.7℃ over $RuNi_1$/AC. It can be inferred that the interaction between Ru and Ni is the most intimate in the $RuNi_1$/AC sample among the samples. However, the reduction peak of $RuNi_2$/AC shifted to a low temperature, 137.4℃, suggesting that the interaction between Ru and Ni was partially weakened at high Ni loading although the reduction peak shows a higher peak than that of Ru/AC. It is also evidenced by the single X-ray diffraction peaks arising from Ni in $RuNi_2$/AC. Therefore, it is inferred that the molar ratio of Ru and Ni affects the interaction between Ru and Ni species over the catalysts.

Figure 2.4 XPS spectra of mono and bimetallic Ru-Ni supported AC in the Ru3p region.

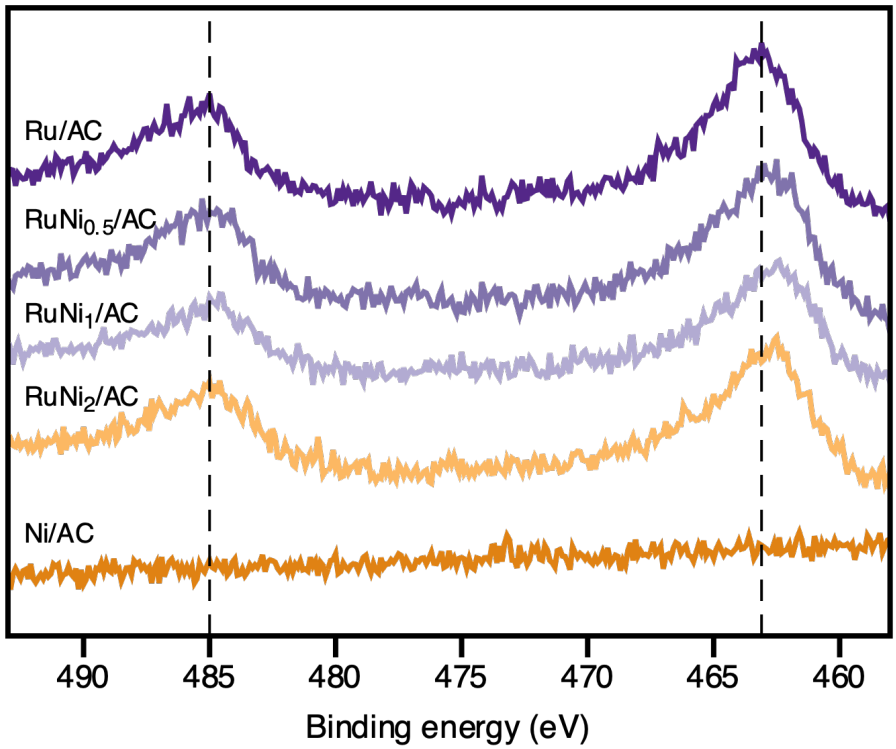

Scheme 2.1 A plausible model of the dissociation and adsorption of hydrogen improved by electronic interaction between Ru and Ni.

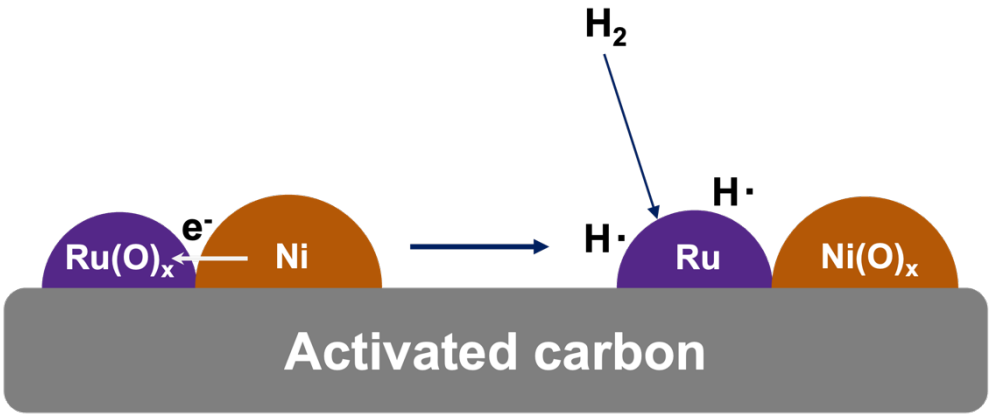

The close contact between Ru and Ni was also confirmed by electron transfer in the XPS spectra of the catalysts as shown in Figure 2.4. Note that the overlap of the Ru3d peak with the C1s peak makes it difficult to investigate the electron transfer between Ru and Ni from the Ru3d peak. It is observed negative shifts for oxidized Ru species in Ru3p spectra when the loading amount of Ni was increased, indicating that electron transfer from Ni to Ru occurs [37]. Considering that the electronegativity of Ru is 2.3, whereas that of Ni is 1.9, this result is feasible. Especially, the biggest negative shift (ca. 0.7 eV) arises as Ni/Ru molar ratio is 1. It is consistent with the previous H_2-TPR analysis (Figure 2.3). A plausible mechanism for the electronic interaction between Ru and Ni on the dissociation and adsorption of hydrogen is depicted in Scheme 2.1. When Ru and Ni are co-impregnated in an appropriate ratio, the Ru species becomes more metallic, which has a positive effect on the catalytic activity of the hydrogenolysis. Indeed, it is well-known that on the metallic Ru surface, hydrogen molecule is dissociated into hydrogen atoms, which in turn participate in the surface reaction [38].

Figure 2.5 Carbon yield during the hydrogenolysis of alginic acid as a function of the reaction parameters such as (a) reaction time (at 210 ℃ under 50 bar H_2 in 100 mM NaOH solution), (b) reaction temperature (for 2 h under 50 bar H_2 in 100 mM NaOH solution), (c) hydrogen pressure (at 210 ℃ for 2 h in 100 mM NaOH solution) and (d) NaOH concentration (at 210 ℃ for 2 h under 50 bar H_2). Product notation: EG = ethylene glycol, PG = 1,2-propanediol, BDO = 1,2-butanediol, TOL = tetritols (erythritol and threitol), POL = pentitols (xylitol, arabitol, and adonitol), LA = lactic acid, GA = glycolic acid, FA = formic acid.

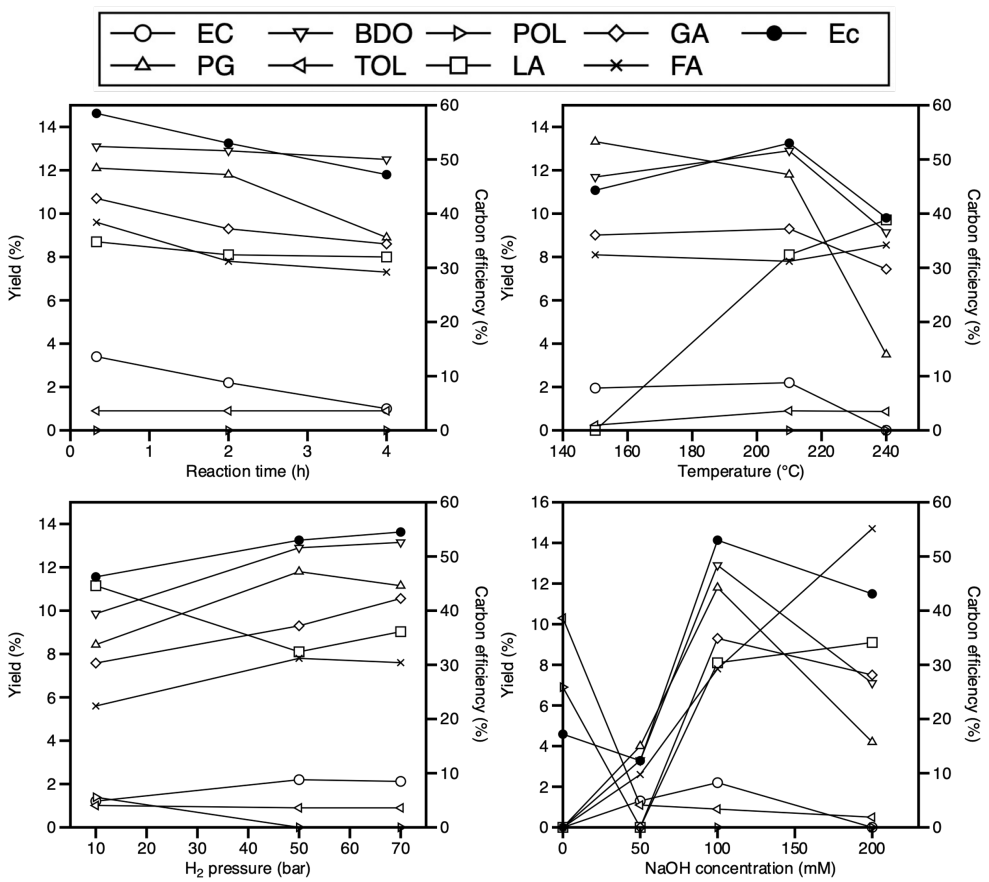

2.3.2. Reaction parameters for hydrogenolysis of alginic acid

The average molecular weights of alginic acid were calculated by GPC analysis. The number average (M_n) and the weight average (M_w) are 72 kDa and 421 kDa, respectively (not shown). Thus, polydispersity index (PDI, M_w/M_n) value of alginic acid is 5.88, which means a measure of the width of the molar mass distribution. It suggests that the molar mass distribution of alginic acid has a very wide molar mass range. However, this trend does not have a significant effect in the decomposition reaction of alginic acid under subcritical conditions [39]. Figure 2.5 presents the changes in various products as a function of reaction parameters including reaction time, temperature, hydrogen pressure, and base concentration over Ru/AC. As shown in Figure 2.5(a), the production of glycols was detected even in a relatively short reaction time. Note that the changes in the amount or distribution of the product were insignificant as the reaction time increased. Such a result was in line with a previous study, which reported that alginic acid sodium salt instantaneously decomposed into organic acids at high pH [11].

As demonstrated in Figure 2.5(b), the yield of glycols did not differ significantly depending on the reaction temperature, whereas organic acids, especially lactic acid (LA), which was not produced at

150 ℃, were produced significantly at 210 ℃. Under the conditions at 210 ℃, the improved carbon efficiency (E_c) yielding value-added products is an encouraging result. However, at temperatures above 210 ℃, unidentified by-products were produced more abundantly. Therefore, the optimum reaction temperature was determined to be 210 ℃, at which E_c increased with a stable yield of glycols.

Hydrogen pressure is also one of the important parameters that influence the conversion of alginic acid (Figure 2.5(c)). LA was predominantly produced compared with other products at 10 bar H_2 pressure. An increased H_2 pressure led to a decrease in the yield of LA with a simultaneous increase in the yield of EG, PG, and BDO. However, when the pressure was higher than 50 bar, the extent of product distribution decreased. Based on this result, the optimum hydrogen pressure was found to be 50 bar.

As shown in Figure 2.5(d), the product yield as a function of NaOH concentration has a large effect on the change in the products. Fewer amounts of glycols and organic acids were produced in the 50 mM solution of NaOH, which is similar to the concentration of alginic acid (52 mM). It can be assumed that the low yield of glycols and organic acids in 50 mM NaOH solution is because alginic acid is titrated with NaOH resulting in few free bases for hydrogenolysis. Increasing the NaOH concentration to 100 mM led to a significant

increase in the yield of glycols, which means that free bases participated in the hydrogenolysis reaction for C-C cleavage. However, in the case of 200 mM solution of NaOH, the yield of glycols decreased whereas the yield of organic acids, especially LA, increased compared with 100 mM NaOH. Various organic acids from alginic acid may exist in the form of salts under basic conditions. Maris et al.[40] reported that LA in the presence of a base can lead to the formation of lactate salt, resulting in the suppressed production of PG during the hydrogenolysis of glycerol. In our results, it was found that the amount of LA produced was proportional to the NaOH concentration, suggesting that sodium lactate converted from free LA inhibited the production of glycols, especially PG. However, the retro-aldol reaction related to the hydrogenolysis process is promoted by adsorbed hydroxyl groups under basic conditions [40]. Hence, the 100 mM NaOH solution, which yields the most glycols, is favorable in the hydrogenolysis although organic acid salts inhibit the production of glycols.

Table 2.2 Product yields and carbon efficiency obtained during the hydrogenolysis of alginic acid over Ru/AC with various basic promoters.

Entry	Catalyst	Base	Liquid-product yield (%)								Other[b] (%)	E_c (%)
			EG	PG	BDO	TOL	POL	LA	GA	FA		
1	none	NaOH	0	0	2.5	0.2	0.3	24.7	0	26.9	25.1	54.6
2	Ru/AC	none	0	0	0	10.3	6.9	0	0	0	49.7	19.4
3	Ru/AC	NaOH	2.2	11.8	12.9	0.9	0	8.1	9.3	7.8	25.1	53.0
4	Ru/AC	$Ca(OH)_2$	0	0	0	0	0	12.1	0	0	63.4	12.1
5	Ru/AC	$CaCO_3$	2.4	13.1	12.7	1.0	0.4	0	11.7	0	57.6	42.4
6	Ru/AC	$Mg(OH)_2$	2.1	11.0	3.6	0.5	0.3	6.7	0	0	37.7	25.5

2.3.3. The role of metal and base for hydrogenolysis of alginic acid

The hydrogenolysis of alginic acid was performed to investigate the role of the metal catalysts and the basic promoters under optimum reaction conditions. As shown in Table 2.2, the presence or the absence of Ru/AC and the basic promoters caused a large change in product distribution. The total carbon yield, which is the sum of by-products calculated by TOC and E_c, does not add up to 100% due to unidentified liquid-products. The depolymerization of alginic acid under basic conditions proceeds to lead the formation of various products. For instance, methanol might be produced in the process of hydrogenolysis. Liu et al.[41] and Lazaridis et al.[42] suggested that methanol is produced via the C-C cleavage of polyols. However, methanol could not be quantified due to technical limitations in our HPLC analysis although it was confirmed that methanol was qualitatively produced.

In addition to methanol, various polyols and organic acids may be formed. The addition of NaOH without Ru/AC resulted in the formation of LA and FA without producing glycols. This is in line with the previous study demonstrating the effect of pH on the conversion of alginic acid sodium salt resulting in the instantaneous formation of organic acids from alginic acid sodium salt at high pH [11].

However, when the reaction was conducted over Ru/AC without the basic promoters, no liquid-products containing fewer than three carbon species were detected resulting in the production of C_4 and C_5 sugar alcohols. Hausoul et al.[43] claimed that C-C cleavage occurs at the end of the carbon chain via decarbonylation rather than the retro-aldol reaction that leads to C_2/C_4 and C_3/C_3 fragments when Ru/AC is used in the hydrogenolysis of sorbitol under neutral or acidic conditions. Accordingly, it is suggested that C_4 and C_5 alcohols were formed via decarbonylation of C_6 sugar alcohols generated via hydrolytic hydrogenation of alginic acid under neutral conditions. Furthermore, it was also confirmed that the decomposition pathway under the conditions occurred via decarbonylation since no product of alcohols below C_4 was detected.

The addition of both metal catalysts and basic promoters led to produce various organic acids and shorter chain polyols such as glycols and BDO, whereas C_4-C_6 sugar alcohols were hardly produced. Likewise, the base promoters play an important role in reducing the amount of unnecessary by-products, which leads to improved E_c. As a result, it can be inferred that the decomposition of alginic acid proceeded via other pathways rather than the decarbonylation reaction. Following the addition of other basic promoters, alginic acid was partially converted to short-chain

polyols except for $Ca(OH)_2$, which lacked the activity for hydrogenolysis. However, $CaCO_3$ and $Mg(OH)_2$ were not appropriate as promoters due to their low carbon efficiencies of 42.4% and 25.5%, respectively. In other words, it is attributed to the larger production of unidentified products than the one with NaOH.

As shown in entries 1 and 3 in Table 2.2, the addition of the Ru catalyst to the NaOH solution altered the distribution and amount of the products by changing the hydrogenolysis pathway. Niemela et al.[44] claimed that the decomposition of alginic acid to organic acids in the alkaline solution proceeds via direct degradation at the end of the chains or cleavage of internal glycosidic linkages. Our results demonstrate that the NaOH promoter has a large effect on both ends and insides of the chain, resulting in the production LA and FA. Furthermore, the basic promoter and catalyst showed a synergistic effect on the production of C_2 compounds such as GA and EG. The selectivity to LA and FA was reduced leading to the production of short-chain polyols. When Ru/AC was used with the NaOH promoter, the yield of by-products was 25.1%, which was approximately half and yield of by-products (49.7%) generated by Ru/AC in a neutral solution. Thus, the suppression of by-products is a significant synergistic effect of the Ru/AC catalyst in the presence of the NaOH promoter.

Figure 2.6 Carbon yield and glycol selectivity during the hydrogenolysis of alginic acid over the catalysts as a function of the Ni/Ru molar ratio. Reaction conditions: at 210 ℃ for 2 h under 50 bar in 100 mM NaOH solution; Product notation: EG = ethylene glycol, PG = 1,2-propanediol, BDO = 1,2-butanediol, TOL = tetritols (erythritol and threitol), POL = pentitols (xylitol, arabitol, and adonitol), LA = lactic acid, GA = glycolic acid, FA = formic acid; [a] Glycol selectivity (%) = (Y_{EG} + Y_{PG}) / (Y_{EG} + Y_{PG} + Y_{BDO} + Y_{TOL} + Y_{POL} + Y_{LA} + Y_{GA} + Y_{FA}) × 100, [b] 8.8 wt% Ru/AC (50 mg) + 5.9 wt% Ni/AC (50 mg).

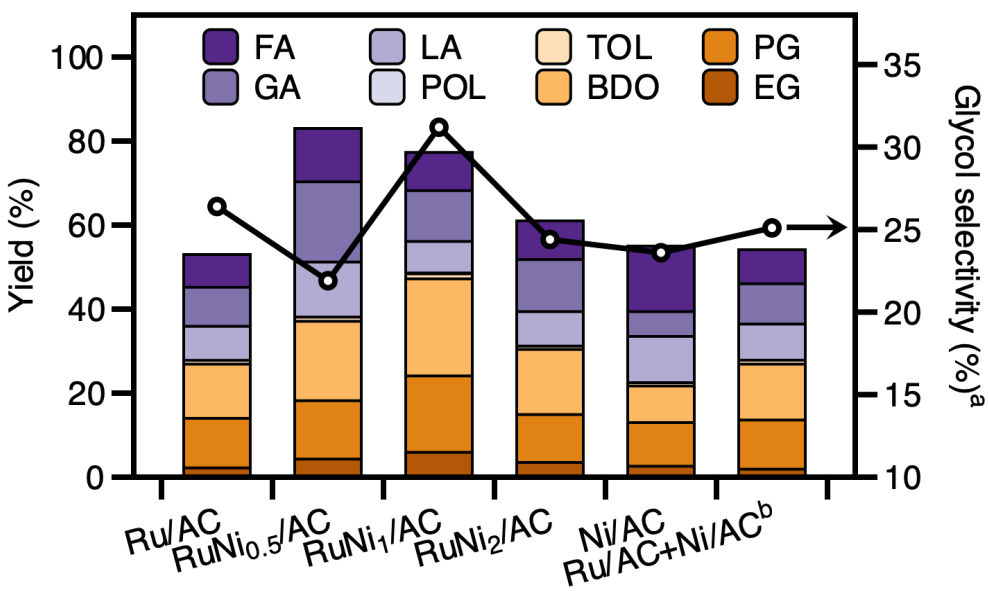

2.3.4. Effect of bimetallic Ru/Ni-based catalysts

Bimetallic Ru/Ni supported on activated carbon catalysts were prepared to further enhance the production of glycols. As shown in Figure 2.6, Ru/Ni bimetallic catalysts show enhanced catalytic activity compared with Ru or Ni monometallic catalysts and physically mixed Ru and Ni catalysts. In case of $RuNi_{0.5}$/AC, the glycol yield and E_c increased significantly from 14.0% to 18.2% and from 53.0% to 83.0%, respectively, compared with Ru/AC. It is reasonable to claim that the hydrogenolysis of alginic acid was more active in the presence of bimetallic catalysts. When the Ni/Ru molar ratio was 1:1, the yield of and selectivity to glycols and BDO were the highest even though E_c decreased slightly. However, the addition of Ni exceeding the Ni/Ru molar ratio of 1:1 resulted in a decrease in the yield of glycols and BDO compared with $RuNi_1$/AC. Based on the results of H_2-TPR with the Ru/Ni bimetallic catalysts (Figure 2.3), the metal reduction peak in $RuNi_1$/AC shifted to the highest temperature among all the catalysts suggesting a strong interaction between Ru and Ni species. In addition, the result obtained from XPS as shown in Figure 2.4 suggests that electron transfer is more likely to occur from Ni to Ru. Hence, the intimate interaction is expected to influence the yield of and selectivity to glycols during the

hydrogenolysis of alginic acid.

Physically mixed Ru/AC and Ni/AC was prepared for investigating the effect of the Ru/Ni interaction on the reactivity. Ru/AC used for physical mixing contains about 8.8 wt% Ru as evidenced by ICP-AES, which is well-dispersed on the activated carbon based on the HAADF-STEM image (not shown). Ru/AC and Ni/AC were mixed physically at a 1:1 ratio, which is similar to the amount of Ru and Ni loaded in $RuNi_1$/AC, suggesting that the bimetallic structure of Ru and Ni is truly effective. Hence, the bimetallic Ru/Ni species, which was formed well when at a Ni/Ru molar ratio of 1:1, most actively promoted the conversion of alginic acid to glycols via hydrogenolysis.

Figure 2.7 Product yields and conversions obtained during the hydrogenolysis of reaction intermediates over Ru/AC in the NaOH solution. Reaction conditions: at 210 ℃ for 2 h under 50 bar in 100 mM NaOH solution; Product notation: EG = ethylene glycol, PG = 1,2-propanediol, BDO = 1,2-butanediol, TOL = tetritols (erythritol and threitol), POL = pentitols (xylitol, arabitol, and adonitol), LA = lactic acid, GA = glycolic acid, FA = formic acid.

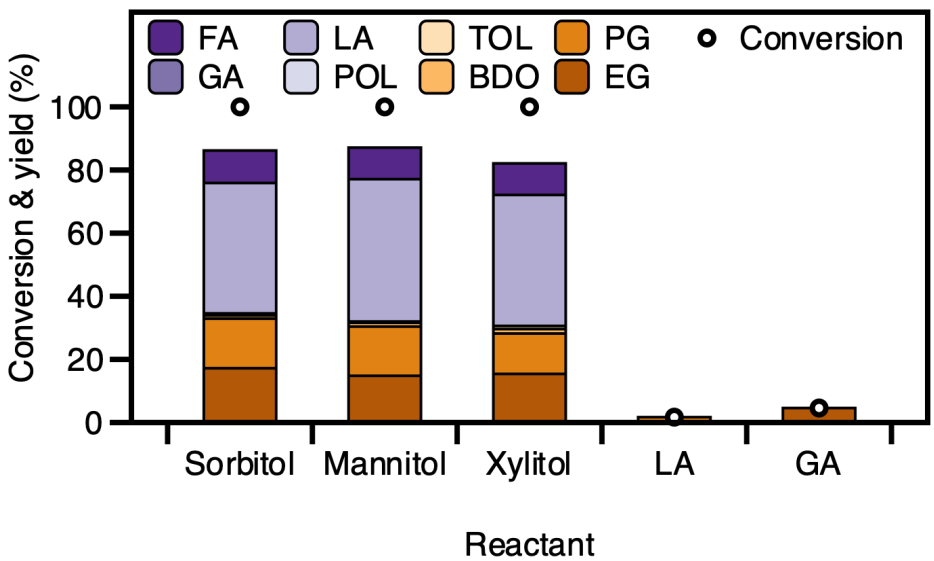

Table 2.3 Product selectivity obtained by the sum of identified liquid-products during the hydrogenolysis of alginic acid and sugar alcohols.

Reactant	Product selectivity (%)	
	EG	PG
Alginic acid	4.2	22.3
Sorbitol	20.0	18.2
Mannitol	17.0	17.9
Xylitol	18.7	15.6

Scheme 2.2 Pathway for the catalytic hydrogenolysis of alginic acid depending on the catalytic conditions. Product notation: EG = ethylene glycol, PG = 1,2-propanediol, BDO = 1,2-butanediol, TOL = tetritols (erythritol and threitol), POL = pentitols (xylitol, arabitol, and adonitol), HOL = hexitols (sorbitol, mannitol, and galactitol), LA = lactic acid, GA = glycolic acid, FA = formic acid.

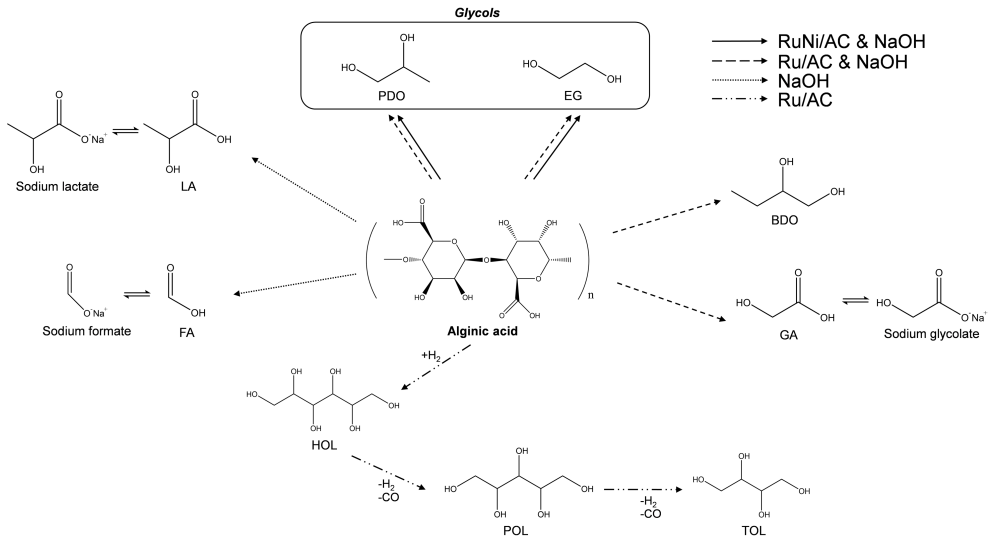

2.3.5. Reaction pathways derived from the hydrogenolysis of intermediates

The following assumptions can be made regarding the reaction pathway of the hydrogenolysis of alginic acid when Ru-based catalysts were used with the NaOH promoter.

First, the polyols are produced via hydrogenolysis of C_6 sugar alcohols, such as sorbitol and mannitol, as intermediates. As shown in Figure 2.7, sugar alcohols, which can be regarded as the intermediate step in the hydrogenolysis of alginic acid, were converted to shorted polyols and LA. In addition, the conversion of all the sugar alcohols was determined to be 100%. However, the EG-to-PG ratio generated from the sugar alcohols was about 1:1 whereas the ratio derived from alginic acid was about 0.2:1 (Table 2.3). Besides, BDO was rarely produced compared with the one from alginic acid, suggesting that it is not mediated via sugar alcohols obtained by the hydrolytic hydrogenation of alginic acid in the production pathway of glycols. Hence, the first assumption can be excluded.

The second assumption is that the polyols are produced via hydrogenation of organic acids depolymerized from alginic acid. However, the organic acids were hardly reactive under severe

hydrogenolysis reaction conditions, resulting in the reduced conversion of LA and GA (1.7% and 4.6%, respectively) as demonstrated in Figure 2.7. Therefore, organic acids do not act as intermediates in the process of glycol production.

Third, glycols and organic acids are produced via separate reaction pathways. As demonstrated in Figure 2.7, hydrogenolysis of sugar alcohols support the third assumption. Although the carbon number between HOL and POL differs, the changes in the selectivity to and yield of LA and FA were insignificant, suggesting that organic acids were obtained via a side effect in the hydrogenolysis of alginic acid in the basic solution. However, Ru/AC with the basic promoter is required for the selective hydrogenolysis to obtain glycols from alginic acid. Thus, it can be suggested that glycols and organic acids were produced via separate reaction pathways, which affect the hydrogenolysis of alginic acid into glycols and organic acids depending on the reaction parameters related to metals and basic promoters rather than the reaction time and temperature.

Therefore, the pathway of alginic acid hydrogenolysis depending on the catalytic conditions can be proposed as shown in Scheme 2.2. Ru/AC in a neutral solution undergoes hydrogenation of alginic acid to HOL, followed by conversion to POL and TOL via decarbonylation. However, further decarbonylation of TOL rarely occurred resulting in

the lack of production of shorter polyols such as EG, PG, and BDO. In the presence of NaOH solution without Ru/AC, alginic acid is converted to organic acids, mainly LA and FA. However, alginic acid decomposed into various organic acids including GA and short-chain polyols such as glycols and BDO over Ru/AC in the presence of NaOH solution. Such organic acids from alginic acid may exist in the form of sodium salts inhibiting the conversion to glycols. The use of a basic solution alters the reaction pathway from decarbonylation to retro-aldol reaction. Glycols, the target products, are produced directly via internal C-C bond cleavage, suggesting that sugar alcohols or organic acids do not act as intermediates during the hydrogenolysis of alginic acid to glycols. Furthermore, bimetallic Ru/Ni supported on activated carbon promotes the hydrogenolysis of alginic acid resulting in increased yield of and selectivity to glycols and E_c.

Chapter 3. Improving the efficiency of Ru metal supported on SiO_2 in liquid-phase hydrogenation of gluconic acid by adding activated carbon

3.1. Introduction

In the current petroleum-based society, various factors such as environmental pollution and price volatility of crude oil have become key motives for finding alternative renewable energy sources over the last decade. A biorefinery is a facility that converts biomass feedstock to biofuels, power, and various value-added chemicals [45-47]. This conversion process is regarded as more sustainable than the petroleum-based refinery, but the processing efficiency should be improved further for its success. In particular, the efficiencies of heterogeneous catalysts applied in biorefineries are an important factor that needs to be improved [48, 49]. Notably, one noble metal is used in the heterogeneous catalytic system to effectively activate the liquid-phase hydrogenation of biomass-

derived compounds, despite its high cost [50-52]. A transition metal that can be used as an alternative to the noble metal suffers from facile deactivation arising from leaching and sintering [53, 54]. Hence, the high utilization efficiency of noble metal-supported catalysts makes them excellent contributors to the development of biorefineries, providing an economic incentive to produce highly value-added chemical products and fuels.

Among various biomass-derived feedstocks, macroalgae contain high levels of structural carbohydrate compounds (approximately 30-50% of dry weight) that can be an abundant carbon source to produce value-added chemicals [6]. Macroalgae, especially brown algae, are cultivated worldwide for use as fertilizers, food, cosmetics, and other products in various industries, and their consumption has continued to increase [55, 56]. Alginic acid extracted from brown algae is a prominent raw material for various chemical building blocks [57]. It consists of L-guluronic acid and D-mannuronic acid connected by β-1,4-glycosidic bonds. These two monomers have a carboxyl group, unlike glucose, which is a unit of cellulose formed by the same glycosidic bond. Thus, it has high potential as a feedstock for biorefinery in terms of product diversity. In biorefineries, alginic acid is converted to sugar alcohols via hydrolytic hydrogenation over Ru-based catalysts [16-18]. In this process, the hydrolysis of alginic

acid into its constituent units, L-guluronic acid and D-mannuronic acid, is mainly promoted by an acid catalyst or H_3O^+ contained in water used as the solvent. Metallic Ru converted the two components to sorbitol and mannitol, respectively, through a successive hydrogenation pathway. In general, hydrogenation using a noble metal catalyst involves hydrogen spillover as a mechanistic step in the reaction, which involves the surface migration of H atoms dissociated by a metal to the support [58-60]. In other words, Ru species play a key role in dissociating molecular hydrogen (H_2) and delivering the H atom to the reactant, and the support provides a site for the surface reaction between the reactant and migrated hydrogen atom.

The so-called interparticle hydrogen spillover refers to the migration of dissociated hydrogen atoms to the adjacent support. The hydrogen migrated from the metal site enables the adjacent support to catalyze the hydrogenation of the reactant, leading to improved metal efficiency. For instance, the quasi-turnover frequency of platinum in benzene hydrogenation over a carbon-supported platinum catalyst increases when it is diluted with pristine carbon [61]. This result suggests that hydrogen spillover to the adjacent carbon, which provides additional adsorption sites for the reactant, is beneficial for improving the catalytic activity of the catalyst system. Lee et al. [62]

performed gas-phase hydrogenation of benzene over Pt-encapsulated LTA zeolites, which have small pores that allow only hydrogen to pass through, to prove the migration of hydrogen atoms between particles. When the Pt catalyst was physically diluted with γ-Al_2O_3, the turnover rate of Pt in benzene hydrogenation was significantly enhanced, indicating that the hydrogen atom dissociated by the Pt spilt-over to γ-Al_2O_3 adsorbed with benzene. The dilution effect in mixed catalytic materials has been confirmed via static volumetric measurements of hydrogen and carbon monoxide uptake [61-63].

Scheme 3.1. Plausible mechanism of water-mediated inter-particle spillover from metal to adjacent support. (a) Dissociation of hydrogen by metal (b) Formation of H_3O^+ species from atomic hydrogen on metal surface (c) Migration of atomic hydrogen from H_3O^+ to adjacent support. Colors: *red*, oxygen; *gray*, hydrogen; *purple*, metal; *blue*, metal-loaded support; *green*, adjacent support without metal.

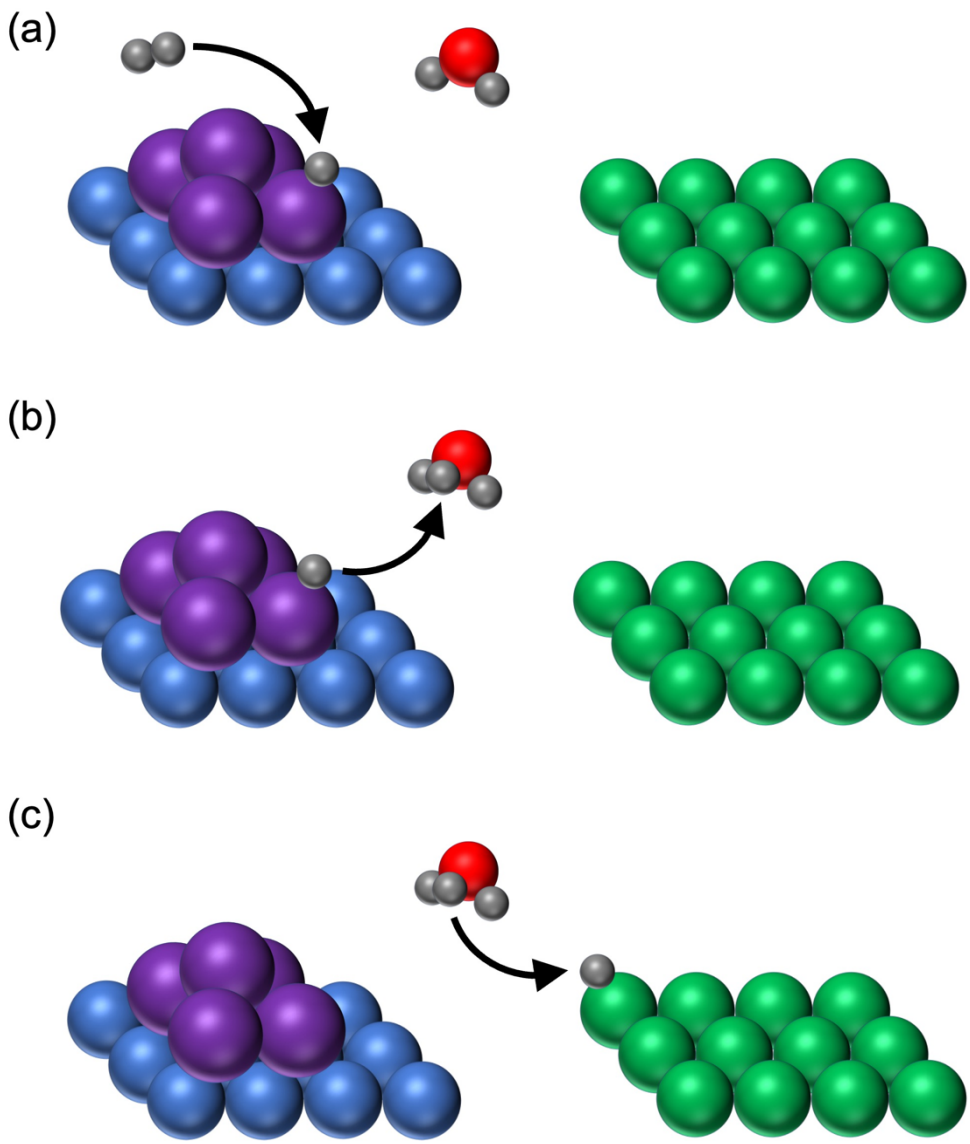

However, studies on the enhancement of the catalytic activity of a metal catalyst in a liquid-phase through interparticle hydrogen spillover have been rarely reported. In the liquid phase, the hydrogen atoms dissociated by the metal equilibrate with the solvated protons and associated electrons at the interface with the solvent, especially water, as illustrated in Scheme 3.1 [64-66]. Subsequently, H_3O^+ species derived from H_2O can transfer atomic hydrogen from the metal surface to the adjacent support [64]. In particular, proton-electron transfer events on Ru clusters, which result in interparticle hydrogen spillover, can occur during the hydrogenation of aldehydes and ketones when polar protic solvents are used [65]. Subcritical and supercritical water has an increased capacity for solvated electrons, and thus the charge imbalance caused by interparticle hydrogen spillover can be resolved [67, 68]. Therefore, we surmised that water-mediated interparticle hydrogen spillover may have a positive effect on the catalytic activity of Ru species in the liquid-phase hydrogenation of reactants.

Scheme 3.2 Target hydrogenation of gluconic acid into sorbitol from hydrolytic hydrogenation pathway of alginic acid.

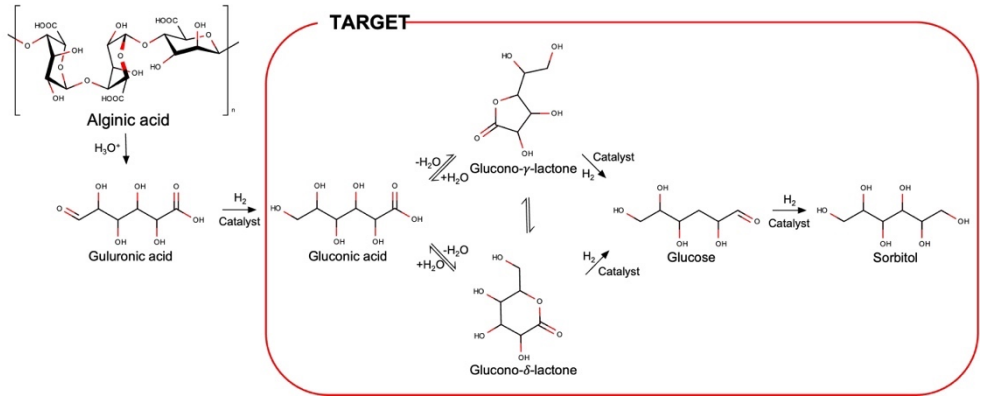

The primary objective of this study was to increase the catalytic efficiency of Ru by mixing a supported Ru metal catalyst with pristine support (same or different type) for liquid-phase hydrogenation. The strategy was to mix the two components without applying a mechanical force to obtain an admixture that could be activated by the interparticle hydrogen spillover mechanism [69]. Gluconic acid (GA), an intermediate in the conversion of alginic acid to sugar alcohols, was used as the reactant (Scheme 3.2). GA is a suitable probe molecule for investigating the hydrogenation of depolymerized compounds derived from the hydrolysis of alginic acid. Under a high pressure, GA is first converted to glucose, and then hydrogenated in successive steps to produce sorbitol. Hence, we performed a two-step cascade hydrogenation of GA into sorbitol using the prepared Ru-supported catalysts in the liquid phase. In addition, several pristine supports, such as activated carbon (AC) and various metal oxides, were mixed with the aqueous reaction solution along with the Ru metal catalyst. Thus, the turnover rate (TOR) of Ru in GA hydrogenation over Ru/SiO_2 mixed with pristine AC was improved without changing the selectivity to sorbitol.

3.2. Experimental sections

3.2.1. Materials and chemicals

Various supports such as AC, SiO_2, and TiO_2 were purchased from Sigma-Aldrich. γ-Al_2O_3 was prepared by calcining Boehmite (Sasol) at 600 ℃ for 22 h. For use as analytical standards, GA (the reactant), glucose, glucono-δ-lactone, and glucono-γ-lactone were purchased from Sigma-Aldrich, except for glucono-γ-lactone procured from Biosynth Carbosynth. Various sugar alcohols such as sorbitol, mannitol, and galactitol were purchased from Alfa-Aesar. The metal precursor, ruthenium chloride hydrate ($RuCl_3 \cdot xH_2O$), and N,O-bis(trimethylsilyl)tri- fluoroacetamide used for derivatizing the liquid product were purchased from Alfa-Aesar. All chemicals were utilized without further purification or treatment, other than that described previously.

3.2.2. Catalyst preparation

The metal precursor, $RuCl_3$, was loaded onto various supports, including AC, SiO_2, TiO_2, and Al_2O_3, by a wet impregnation method. An aqueous solution of $RuCl_3$ (150 mL) was stirred with 2 g of each support for 2 h, followed by evaporation using a rotary evaporator. The concentrated sample was dried overnight in an oven at 105 ℃, and then reduced at 350 ℃ for 2 h using a stream of 5% H_2/N_2 (100

ccm). This was followed by a passivation process under 2% O_2/N_2 gas flow (100 ccm) at room temperature for >3 h. All the prepared catalysts are designated as Ru/S + P, where Ru/S represents the Ru-loaded support and P represents the pristine support added to the Ru/S sample. For example, Ru/SiO_2 + AC represents an admixture of a Ru catalyst supported on SiO_2 added with pristine AC.

3.2.3. Catalyst characterization

To determine the amount of Ru loaded in the prepared catalysts, inductively coupled plasma atomic emission spectroscopy (ICP-AES) was performed using an OPTIMA 8300 instrument (Perkin-Elmer, USA). To investigate the crystallinity of the Ru metal and supports, X-ray diffraction (XRD) was carried out on a Smartlab diffractometer (Rigaku) operated at a current of 30 mA and voltage of 40 kV. The Ru dispersion on the as-prepared catalysts was characterized by volumetric CO chemisorption, assuming a stoichiometric Ru/CO ratio of 1 (ASAP2020PLUS, Micromeritics). For this, the test samples were evacuated at 200 ℃ for 4 h to remove physisorbed species and pretreated under 99.9999% H_2 gas flow at 350 ℃ for 2 h, followed by CO chemisorption at 35 ℃. The surface area (S_{BET}) of each catalyst sample was analyzed by N_2 adsorption and desorption using

ASAP2020PLUS. The samples were degassed at 200 ℃ for 6 h to remove residual water and impurities, and the N_2 adsorption/desorption isotherms were collected at -196 ℃. The particle size and dispersion of Ru on the support were investigated via high-resolution transmission electron microscopy (HRTEM) at an accelerating voltage of 200 kV using a JEM-2100F microscope (JEOL) equipped with a field-emission gun, resulting in a point resolution of 2.3 Å. Energy-dispersive X-ray spectroscopy (EDS) mapping and line-EDS were also performed on the samples to investigate their chemical compositions. Hydrogen temperature-programmed reduction (H_2-TPR) and hydrogen temperature-programmed desorption (H_2-TPD) analyses were performed on a BELCAT-II catalyst analyzer (BEL Japan Inc.) to evaluate the reducibility of the Ru catalysts. For H_2-TPR analysis, the Ru catalyst samples were reduced under 5% H_2/Ar flow (50 cm) at 350 ℃ for 2 h. The samples were then cooled to 50 ℃. After this pretreatment, H_2-TPR curves were acquired while ramping up the temperature from 50 to 900 ℃ (10 ℃/min) under 5% H_2/Ar gas flow (30 ccm). For H_2-TPD analysis, the Ru catalyst (0.2 g) and pristine support (0.2 g) were mixed at a ratio of 1:1 using a vortex mixer (Scilogex MX-S) for sufficient time. The samples were then reduced at 350 ℃ for 2 h under 5% H_2/Ar (50 ccm). Thereafter, the samples were cooled to

100 ℃, followed by H_2 adsorption at 100 ℃ for 30 min using 5% H_2/Ar (50 ccm). After cooling to 50 ℃, the amount of desorbed hydrogen was detected using a thermal conductivity detector, while the sample was heated to 700 ℃ (5 ℃/min) under Ar flow (50 ccm).

3.2.4. Catalytic activity

The hydrogenation of the substrate (GA) was performed in a 100 mL autoclave (Parr Instrument Company) charged with GA (1 wt%), deionized water (30 mL), and the Ru catalyst. For reactions using an admixture of the supported Ru catalyst and pristine support, each powder was added to the reaction mixture without mechanical mixing, such as grinding in a mortar or ball-milling. The reaction was conducted in the range of 80 to 160 ℃ (after ramping at 10 ℃/min rate from room temperature) with stirring (1000 rpm) for 0.3 - 1 h under 50 bar of H_2 after purging the autoclave three times with 99.999% Ar to remove air from it. After the reaction, the liquid product in the reactor, which was rapidly quenched with ice-cold water to prevent further side reactions, was collected manually.

3.2.5. Adsorption test

Adsorption tests were performed at room temperature with stirring at 400 rpm for 3 h in a 10 mL vial charged with a pristine support (100 mg) as the adsorbent and an adsorbate (1 wt% aqueous solution, 2 mL). After the reaction, the liquid product in the vial was filtered to remove the catalyst and analyzed by gas chromatography-flame ionization detector (GC-FID). The adsorbed amount (mmol/g) of the adsorbate was calculated from the difference between the initial and residual quantities of the adsorbate in the solution. When GA was used as the adsorbate, the adsorbed amount was calculated as the sum of GA and gluconolactones (the lactone forms of GA).

3.2.6. Product analysis

All the liquid products were derivatized with N,O-bis(trimethylsilyl)trifluoroacetamide to obtain silylated samples for analysis by GC-FID (Agilent 6890) using a DB-5 column. The silylated GA, glucose, glucono-δ-lactone, glucono-γ-lactone, sorbitol, mannitol, and galactitol derivatives were calibrated using external standards. Additionally, liquid chromatography with tandem mass spectrometry (LC-MS/MS, LC/MS-Q-TOF 5600, AB Sciex, USA) was used for the qualitative analysis of the products. The factors related to the catalytic activity such as conversion,

selectivity, and TOR were calculated as follows:

$$Conversion(\%) = \left(1 - \frac{mol_{GA} + mol_{gluconolactones}}{initialmol_{GA}}\right) \times 100\% \quad (1)$$

$$Selectivity(\%) = \frac{mol_{product}}{\left(1 - \frac{mol_{GA} + mol_{gluconolactones}}{initialmol_{GA}}\right)} \times 100\% \quad (2)$$

$$TOR\left(h^{-1}\right) = \frac{mol_{sorbitol}}{mol_{Ru} \times t} \quad (3)$$

Where mol_{GA}, $mol_{gluconolactones}$, $mol_{product}$, $mol_{sorbitol}$, and mol_{Ru} are the numbers of moles of GA, gluconolactones, sorbitol and Ru, respectively, and t is time (h).

We should note that the TOR values in this study were determined based on the total amount of Ru loaded in the catalyst and not from the amount of reactive surface Ru species calculated by CO chemisorption.

Table 3.1 Summary of various catalyst characteristics.

Catalyst	Loading amount (wt%)	S_{BET} (m^2 g^{-1})	Particle size (nm)	CO chemisorption		
				Uptake (μmol g^{-1})	Dispersion (%)	Particle size (nm)
Ru/AC	5.1	615 (858)	1.9 ± 0.4	362.5	71.8	1.8
Ru/SiO_2	5.3	336 (381)	3.4 ± 0.8	111.8	22.6	5.9
Ru/TiO_2	5.1	59 (59)	2.6 ± 0.4	73.1	14.8	9.0
Ru/Al_2O_3	4.9	177 (180)	3.5 ± 0.5	135.7	27.4	4.0

[a] Analyzed by ICP-AES.

[b] Calculated by BET method. S_{BET} in parentheses were obtained from pristine support without Ru.

[c] Calculated by HRTEM.

Figure 3.1 XRD diffractograms of Ru catalysts (Ru/AC, Ru/SiO_2, Ru/TiO_2, and Ru/Al_2O_3). Symbols: ●, ruthenium (PDF: 06-0663); ▼, carbon (PDF: 26-1080); ■, titania (anatase) (PDF: 21-1272); □, titania (rutile) (PDF: 21-1276); ◆, alumina (PDF: 10-0425).

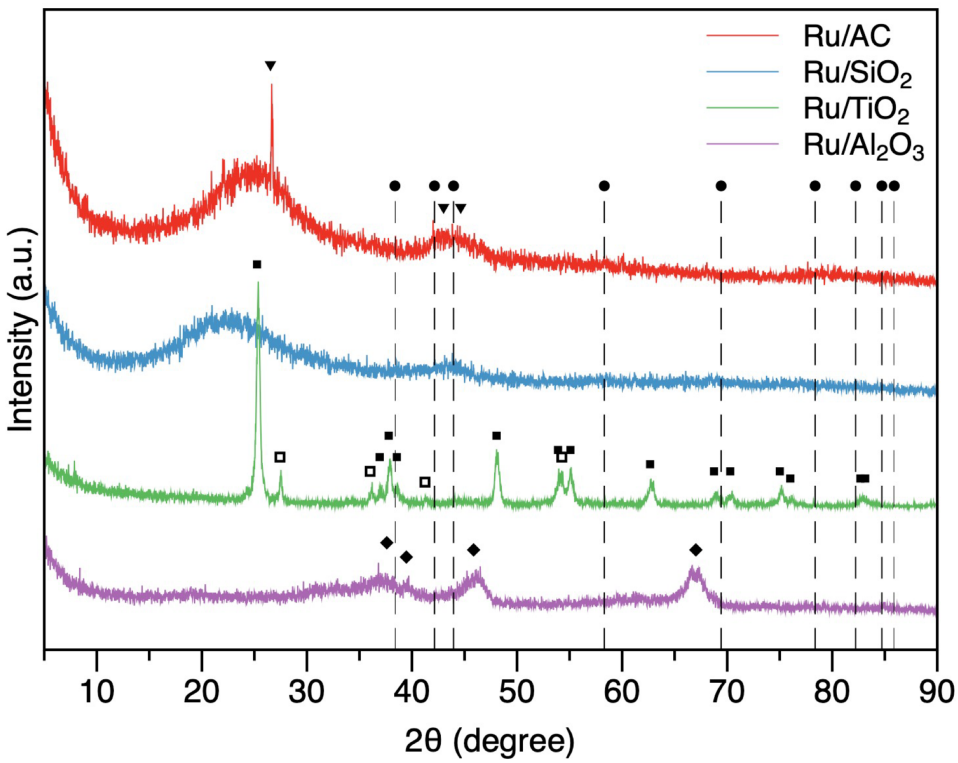

Figure 3.2 HRTEM images of Ru catalysts (a) Ru/AC (b) Ru/SiO_2 (c) Ru/TiO_2 (d) Ru/Al_2O_3 and their particle size distribution.

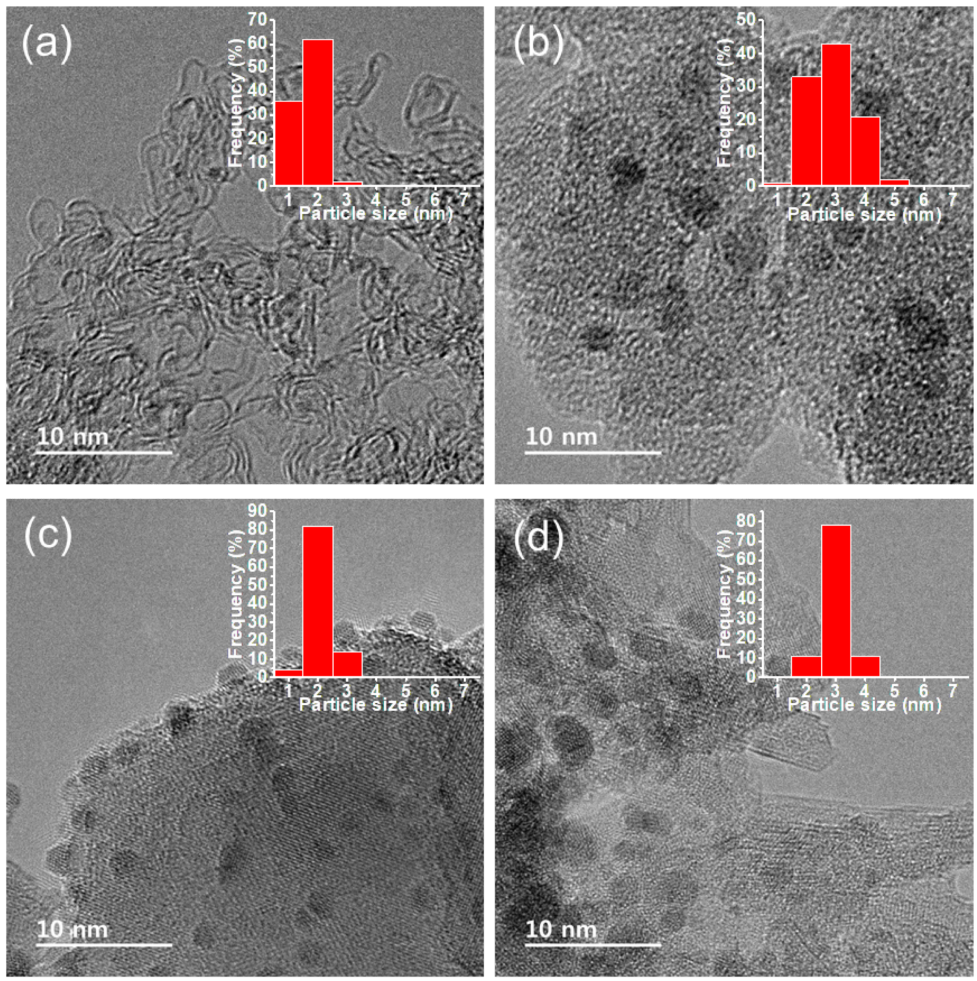

Figure 3.3 H_2-TPR profiles of Ru catalysts (Ru/AC, Ru/SiO_2, Ru/TiO_2, and Ru/Al_2O_3).

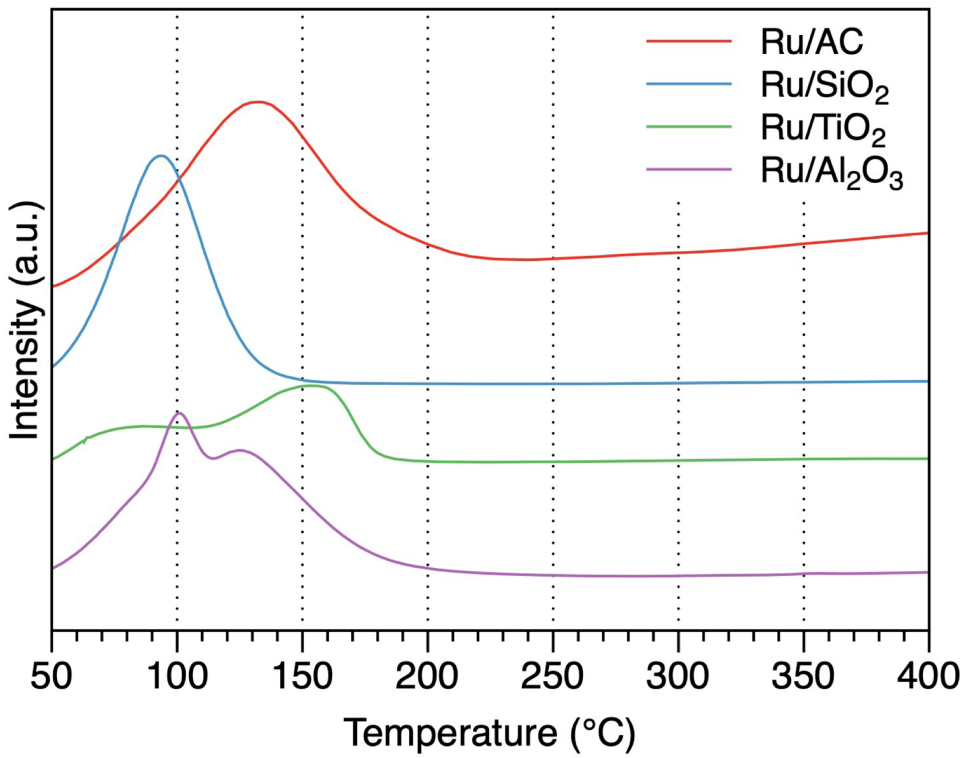

3.3. Results and discussion

3.3.1. Characterization of Ru catalysts

Characterization results of the supported Ru catalysts such as Ru/AC, Ru/SiO_2, Ru/TiO_2, and Ru/Al_2O_3 are summarized in Table 3.1. The amount of Ru loaded in the supported catalyst was consistent with the intended amount of 5 wt%, as determined by ICP-AES. The surface areas of the Ru catalysts determined by N_2 adsorption-desorption analyses were different for different supports, indicating a difference in the pore structure of the supports. In addition, Ru was well-dispersed without the agglomeration of Ru species on the support in all the prepared Ru catalysts, as inferred from the XRD patterns in Figure 3.1, where no specific Ru crystal peaks are detected. Further, the average particle size of Ru on the support surface was analyzed via HRTEM (see Table 3.1 and Figure 3.2). The Ru/AC sample exhibited the smallest Ru particle size (1.9 nm) among the prepared Ru catalysts. Interestingly, in the case of Ru/TiO_2, the Ru particle size obtained from CO chemisorption was significantly larger than the average size observed in HRTEM images, which can be attributed to the decrease in the number of CO adsorption sites on the Ru surface owing to strong metal-support interaction between the Ru particles and TiO_2 [70, 71]. The change

in the peak broadness, peak separation, and the shoulder peak in the H_2-TPR profiles of the Ru catalysts in Figure 3.3 suggest that various Ru species, such as RuO_x, $RuCl_3$, and $RuOCl_2$, were reduced at different temperatures depending on the type of support, suggesting that the reducibility of Ru was influenced by the type of support [72, 73].

Figure 3.4 LCMS of liquid-product from glucono-δ-lactone hydrogenation over Ru/SiO_2. Reaction conditions: 1 wt% glucono-δ-lactone in 30 mL H_2O, 20 mg Ru/SiO_2, 120 ℃, 1 h, 1000 rpm stirring.

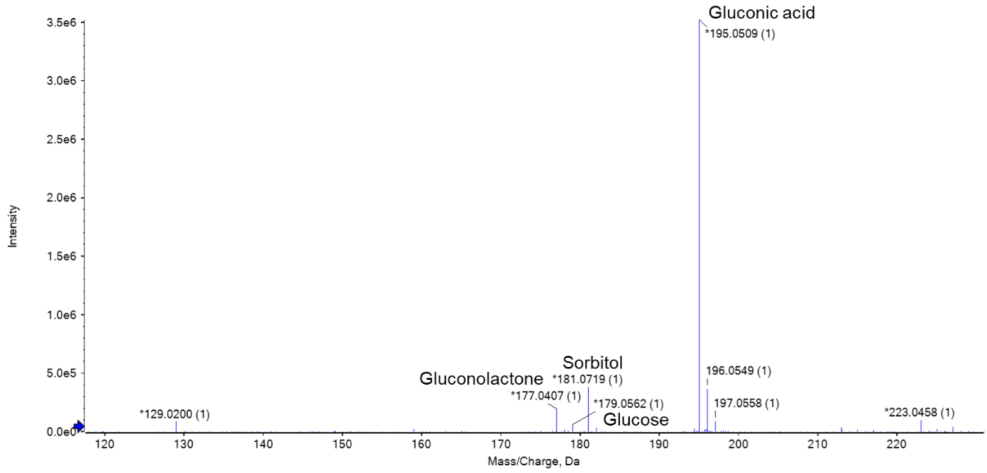

Figure 3.5 Catalytic activity of the Ru catalysts as a function of support in the hydrogenation of gluconic acid to sorbitol. Reaction conditions: 1 wt% gluconic acid in 30 mL H_2O, 20 mg catalyst, 120 ℃, 1 h, 1000 rpm stirring. Conversion: <30%, selectivity: >99%.

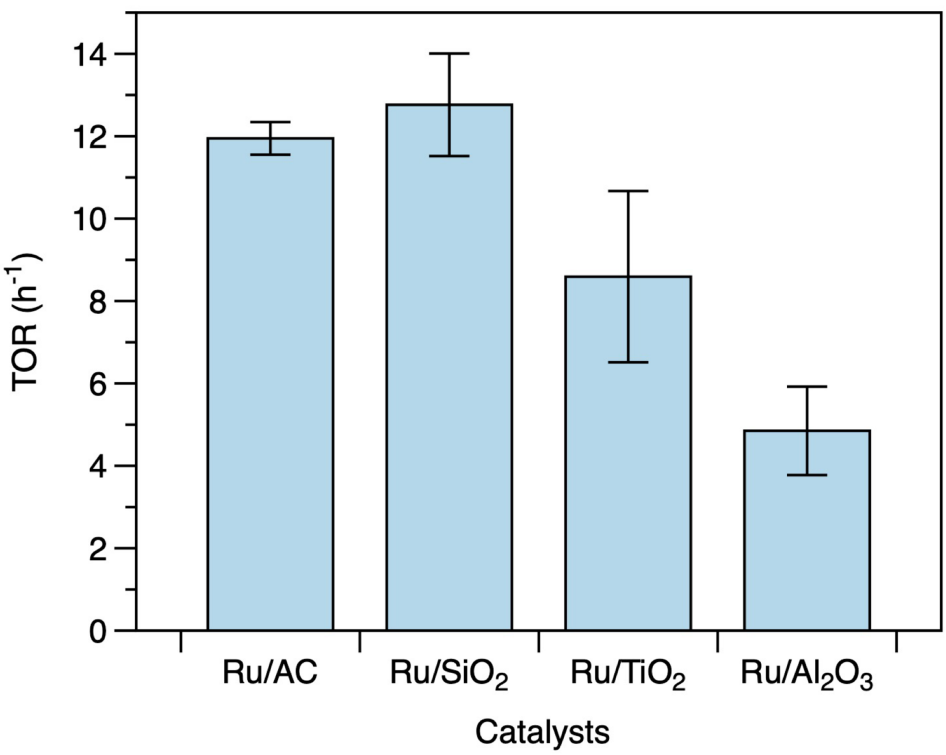

3.3.2. GA hydrogenation over Ru catalysts

The hydrogenation of GA was performed over various catalysts with and without the presence of Ru species under 50 bar of H_2 at 120 ℃ for 1 h. This resulted in the formation of sorbitol as the target product without the generation of other isomers or sugar alcohols such as mannitol, galactitol, and xylitol (not shown). Meanwhile, hydrogenation of glucono-δ-lactone was performed over Ru/SiO_2, which resulted in the detection of GA, glucono-γ-lactone, glucose, and sorbitol as shown in Figure 3.4. This is in an accordance with previous research by Fabre et al. [74] who reported a complete hydrogenation of the two gluconolactones in equilibrium with GA into sorbitol over Ru catalysts. Hence, in an aqueous solution, GA exists in equilibrium with two gluconolactone forms, viz., glucono-δ-lactone and glucono-γ-lactone, depending on the temperature and pH (Scheme 3.2) [74, 75]. When GA hydrogenation was attempted over pristine AC or oxide supports without Ru, only GA and gluconolactone forms were detected without the hydrogenated compounds, such as glucose or sorbitol, as determined by LC-MS/MS (not shown). However, the amount of glucose analyzed by GC-FID was negligible, indicating that glucose was produced as a transient intermediate that was rapidly converted to sorbitol.

Figure 3.5 shows the results of the catalytic hydrogenation of GA to sorbitol over Ru catalysts loaded on various supports, such as AC, SiO_2, TiO_2, and Al_2O_3. The catalytic activity of Ru depended strongly on the characteristics of the supports, which influence the physicochemical properties of Ru metal, such as its reducibility and dispersion [76]. In the previous section, we confirmed that the change in the dispersion and reducibility of Ru depends on the support. Among the supported catalysts, Ru/SiO_2 exhibited the highest TOR, suggesting that SiO_2 is the optimal support for achieving high catalytic efficiency of Ru in GA hydrogenation.

Figure 3.6 Catalytic activity of Ru catalysts (a) Ru/AC, (b) Ru/SiO_2, (c) Ru/TiO_2, (d) Ru/Al_2O_3, mixed with pristine supports in the hydrogenation of gluconic acid to sorbitol. Reaction conditions: 1 wt% gluconic acid in 30 mL H_2O, 20 mg catalyst, 40 mg pristine support, 120 ℃, 1 h, 1000 rpm stirring. Conversion: <30%, selectivity: >99%.

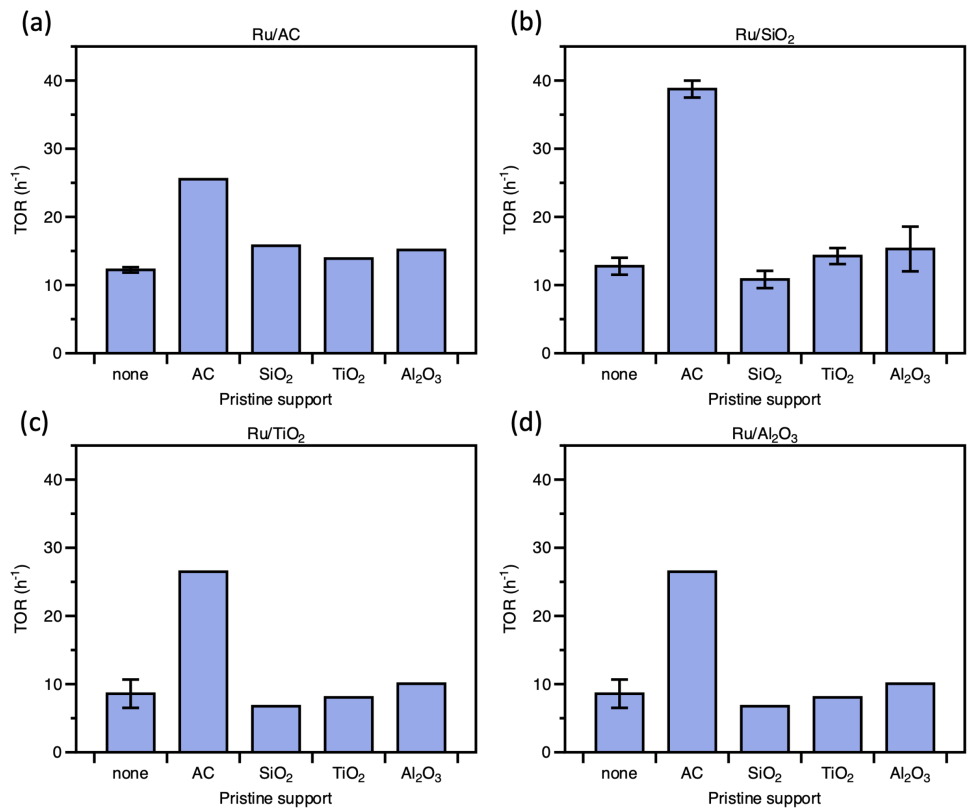

Figure 3.7 Catalytic activity of Ru/SiO_2 mixed with pristine support in the hydrogenation of gluconic acid to sorbitol as a function of reaction temperature. Reaction conditions: 1 wt% gluconic acid in 30 mL H_2O, 20 mg catalyst, 40 mg pristine support, 80-160 ℃, 0.3-1 h, 1000 rpm stirring. Conversion: <30%, selectivity: >99%.

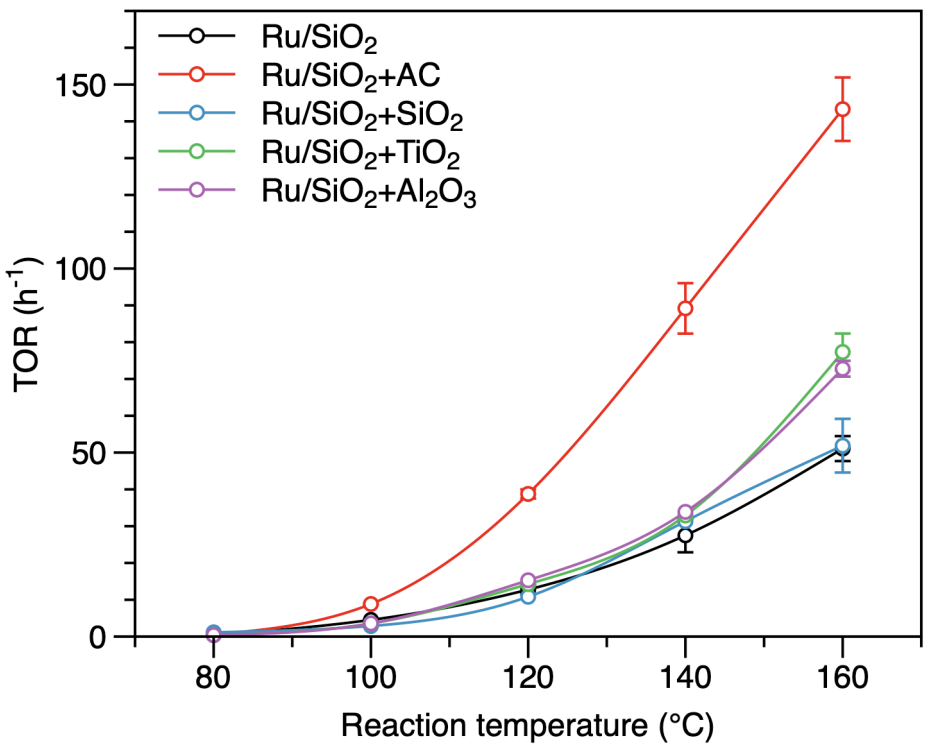

Figure 3.8 Turnover rate of Ru on gluconic acid hydrogenation as a function of added amount of activated carbon to Ru/SiO_2. Reaction conditions: 1 wt% gluconic acid in 30 mL H_2O, 20 mg Ru/SiO_2, 0-80 mg activated carbon, 120 ℃, 1 h, 1000 rpm stirring. Conversion: <30%, selectivity: >99%.

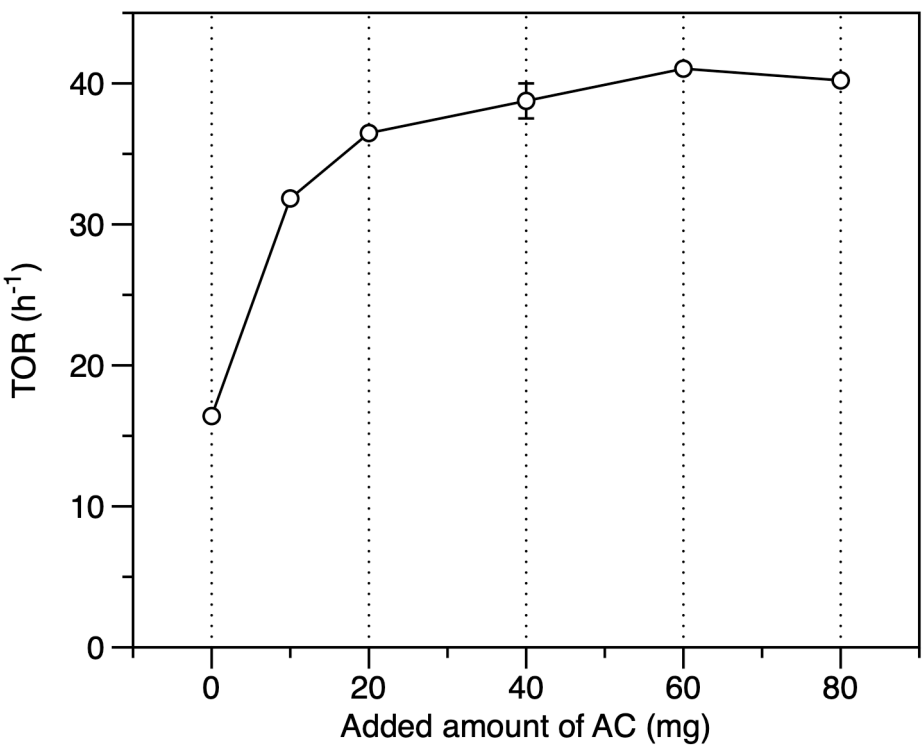

3.3.3. Effect of mixing pristine supports with Ru catalysts on GA hydrogenation

Each of the supported Ru catalyst was mixed with each of the other pristine supports, viz., AC, SiO_2, TiO_2, and Al_2O_3, in an autoclave for GA hydrogenation to evaluate the effects of mixed supports on the catalytic activity of Ru. As illustrated in Figure 3.6(a)–(d), the addition of AC to all supported Ru catalysts led to a significant increase in the TOR of Ru in GA hydrogenation. Given that none of the pristine supports (without Ru) were catalytically active in GA hydrogenation, it can be inferred that pristine AC interacted with the Ru species on the support, thereby promoting the catalytic activity of Ru.

Upon mixing with pristine AC, the TORs of Ru in Ru/TiO_2, Ru/Al_2O_3, and Ru/SiO_2 increased from 8.6 to 26.5 h^{-1}, 4.8 to 30.3 h^{-1}, and 12.8 to 38.8 h^{-1}, respectively. These values are higher than the TOR of Ru in Ru/AC mixed with AC. However, in the absence of AC, the TORs of Ru/TiO_2 and Ru/Al_2O_3 were lower than that of Ru/AC, which indicates the positive effect of mixing AC, irrespective of the support. However, the addition of metal oxides had little effect on hydrogenation. For instance, the TORs of Ru/SiO_2 + TiO_2 and Ru/SiO_2 + Al_2O_3 increased slightly to 14.3 and 15.3 h^{-1}, respectively, while

that of Ru/SiO_2 + SiO_2 decreased to 10.8 h^{-1}. This result strongly suggests that AC is more effective than the metal oxides (SiO_2, TiO_2, and Al_2O_3) in improving the Ru efficiency, when mixed with the Ru catalysts.

Figure 3.7 shows the TOR of Ru as a function of reaction temperature for Ru/SiO_2 and Ru/SiO_2 mixed with pristine supports (Ru/SiO_2 + P). At a low reaction temperature of 80 ℃, both Ru/SiO_2 and Ru/SiO_2 + P, had little effect on GA hydrogenation, indicating that the reaction temperature was insufficient for activating the Ru catalysts. The Ru catalysts, however, became active as the reaction temperature was increased beyond 100 ℃. At 100 ℃, the TOR of Ru in Ru/SiO_2 + AC increased significantly to 8.8 h^{-1}, compared to that of Ru/SiO_2 (4.5 h^{-1}), whereas no promotional effect was induced by other metal oxides. We speculate that the promotional effect of pristine AC mixed with the Ru catalysts can be caused by the activation of Ru species for GA hydrogenation under appropriate experimental conditions. Ru/SiO_2 + AC facilitated a rapid conversion of GA to sorbitol as the temperature increased and exhibited a maximum TOR of 143.3 h^{-1} at 160 ℃. However, when pristine metal oxides were added, the admixtures had little effect on the TOR, although the TiO_2 and Al_2O_3 slightly increased the TOR at the reaction temperature of 160 ℃.

We also performed GA hydrogenation by varying the amount of pristine AC added to the Ru/SiO_2 catalyst (Figure 3.8). As the amount of added AC was increased 10 to 60 mg, the TOR of Ru/SiO_2 increased abruptly. However, the rate of increase gradually slowed and saturated at 80 mg of added AC. It should be noted that hydrogen atoms dissociated by the metal need to travel a longer distance when reactants in the vicinity of the metal particles are already hydrogenated, which can be the rate-determining step [77, 78]. That is, even if the added amount of AC is increased substantially, it is difficult for active hydrogen to be transferred to the surface of all the added AC. Therefore, the optimum amount of pristine AC depends on the amount of Ru in the supported catalyst.

Figure 3.9 H_2-TPD profiles of pristine supports (curve I), Ru/SiO_2 (curve II), Ru/SiO_2 mixed with pristine supports (curve III), and the sum of (curve I) and (curve II). (a) activated carbon, (b) SiO_2, (c) TiO_2, and (d) Al_2O_3 as a pristine support.

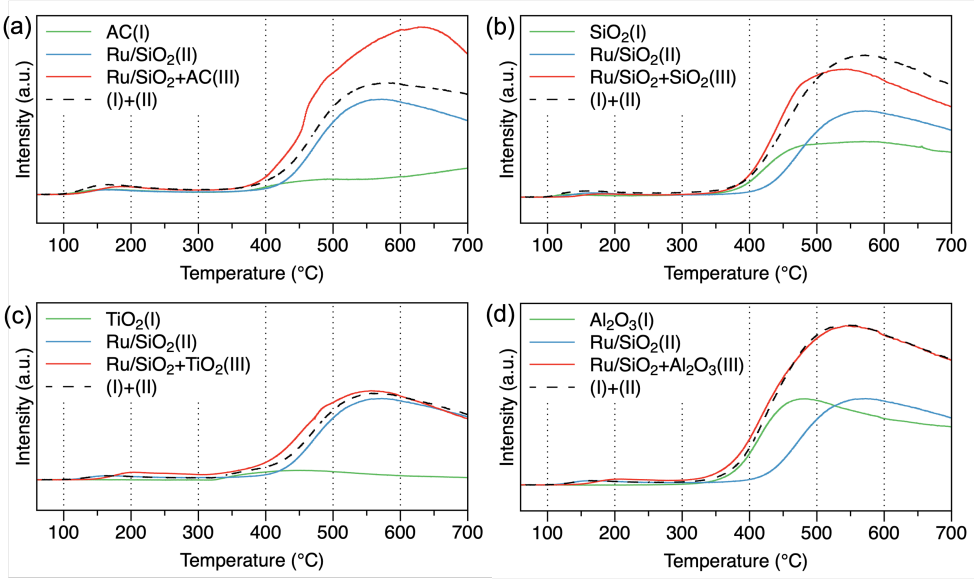

3.3.4. H_2-TPD study on Ru catalyst admixtures

The reaction between GA and hydrogen on the added pristine AC requires the dissociation of molecular hydrogen (H_2), which does not occur in the absence of a metal catalyst such as Ru. That is, Ru species are essential to dissociate the hydrogen molecules into hydrogen atoms [79, 80], indicating that pristine AC uptakes the hydrogen atoms from the Ru catalyst. As H_2O can aid the migration of hydrogen atoms that are chemically adsorbed on the catalyst surface to an adjacent support surface [64-66], we speculate that water-mediated interparticle hydrogen spillover occurs between the Ru catalyst and pristine AC in the aqueous solution (Scheme 3.1). Wisniak et al. [80] claimed that the surface reaction for glucose hydrogenation proceeds between the adsorbed hydrogen atoms and glucose according to the Langmuir-Hinshelwood mechanism at a H_2 high pressure, suggesting that the adsorption of both the reactants is critical for the added pristine AC to activate the hydrogenation of the reactant, as discussed later.

H_2-TPD analysis was performed to further investigate the hydrogen adsorption and desorption characteristics of the catalyst surface. All the pristine supports, Ru/SiO_2, and Ru/SiO_2 + P were analyzed by H_2-TPD. It is well known that Ru catalysts exhibit two

hydrogen desorption peaks at different temperatures, indicating the presence of two types of hydrogen species on them [81, 82]. As shown in Figure 3.9, although weak peaks that are usually assigned to chemisorbed hydrogen on the Ru surface were observed below 200 ℃, we ignored them because the differences in the peak intensities between the samples were negligible. However, significant hydrogen desorption peaks were observed above 400 ℃, which are attributed to spilt-over hydrogen associated with the support (in our case, SiO_2) containing Ru or the adjacent pristine support mixed with the Ru catalyst. Meanwhile, pristine supports, especially SiO_2 and Al_2O_3, also exhibited H_2 desorption peaks at temperatures above 400 ℃. This could be attributed to the non-reducible nature of SiO_2 and Al_2O_3, resulting in stronger adsorption of hydrogen than to reducible supports such as AC and TiO_2 [83].

As shown in Figure 3.9(a), the amount of hydrogen desorbed in the high temperature range from Ru/SiO_2 + AC (curve III) was significantly higher than the sum of the amounts of hydrogen desorbed individually from AC (curve I) and Ru/SiO_2 (curve II). This result strongly indicates that interparticle hydrogen spillover occurred from Ru/SiO_2 to pristine AC in the mixed sample, Ru/SiO_2 + AC. However, when pristine metal oxides were mixed with Ru/SiO_2, there was negligible difference in the amount of desorbed hydrogen

compared to the sum of individual curves (Figure 3.9(b)-(d)). This suggests that no activation of added oxides via interparticle hydrogen spillover occurred owing to weak interactions between Ru/SiO_2 and pristine metal oxides, consistent with the insignificant effect of mixing pristine metal oxides and Ru/SiO_2 on GA hydrogenation. Hence, the effect of the added pristine support is possibly related to its ability to uptake the atomic hydrogen from the Ru species. Among the various pristine supports, AC could additionally uptake the spilt-over hydrogen, rather than the other metal oxides, through physical contact with Ru/SiO_2. Remarkably, water can play an important role as a mediator between Ru species and AC in the liquid phase, where physical contact between solid components is difficult. Therefore, we believe that the ability to uptake the spilt-over hydrogen on AC can also work in liquid-phase hydrogenation.

Table 3.2 Adsorbed amounts on various pristine supports obtained from adsorption test of GA and glucose.

Support	Adsorbed amount (mmol/g)[a]	
	GA	Glucose
AC	0.50	0.34
SiO_2	0.05	0.02
TiO_2	0.25	0.01
Al_2O_3	0.31	n. d.

[a] Analyzed by adsorption test. Adsorption test conditions: 1 wt% gluconic acid or glucose as an adsorbate in 2 mL H_2O, 100 mg pristine support as an adsorbent, RT, 3 h, 400 rpm stirring.

Figure 3.10 Adsorbed amount of (a) gluconic acid and (b) glucose measured from adsorption tests as a function of mixed amount of activated carbon to Ru/SiO_2. Adsorption test conditions: 1 wt% gluconic acid or glucose as an adsorbate in 2 mL H_2O, 20 mg Ru/SiO_2 and 0-80 mg activated carbon as an adsorbent, room temperature, 3 h, 400 rpm stirring.

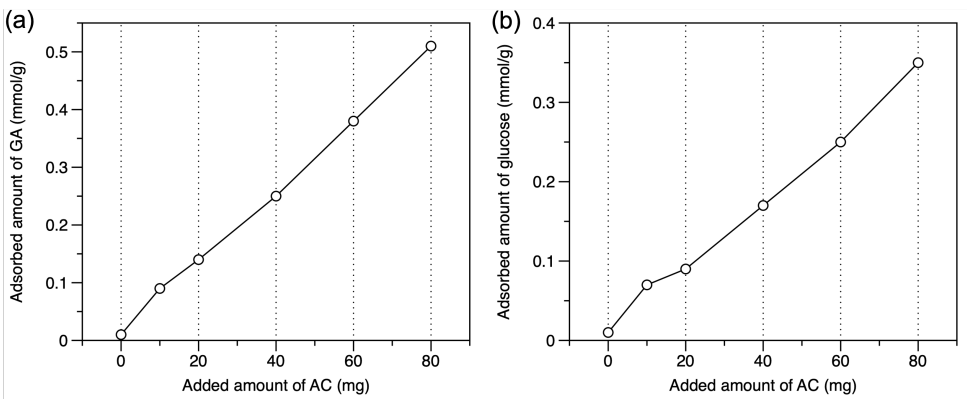

3.3.5. Adsorption properties of pristine supports

As mentioned above, the added pristine support should contain sufficient adsorption sites for the reactant as well as for hydrogen. Therefore, we investigated the adsorption of GA and glucose (which is an intermediate in GA hydrogenation) as adsorbates on various pristine supports. Although the amount of adsorbed reactant cannot be directly correlated with the catalytic activity, it indicates the affinity of the support surface to the reactant [84].

As shown in Table 3.2, the amounts of GA and glucose adsorbed on AC were 0.50 and 0.34 mmol/g, significantly higher than the amounts adsorbed on the other metal oxides. The high affinity of pristine AC to the reactants indicates that pristine AC provides additional active sites for hydrogenation. Such reactant affinity is attributed to the presence of hydrophilic functional groups and the large surface area on the AC surface (Table 3.1) [84, 85]. In other words, the water-soluble GA can easily access the AC surface in water utilized as the solvent. Therefore, it can be concluded that the hydrogenation of GA with spilt-over hydrogen atoms adsorbed on pristine AC can occur. In this regard, water can play a critical role in interparticle hydrogen spillover from Ru onto pristine AC, and also the adsorption of GA on pristine AC.

In the case of TiO_2 and Al_2O_3, the adsorbed amounts of GA were moderate at 0.25 and 0.31 mmol/g, respectively, but those of glucose were extremely low. SiO_2 had the smallest adsorbed amounts of GA and glucose at 0.05 and 0.02 mmol/g, respectively, although Ru/SiO_2 exhibited the highest TOR among the prepared Ru catalysts. Note that GA hydrogenation to produce sorbitol can proceed on the surfaces of both Ru and the support [43]. Hence, the adsorption results indicate that pristine metal oxides are unable to provide sufficient adsorption sites for both hydrogen and reactants compared to AC, resulting in the absence of the mixing effect on GA hydrogenation over Ru/SiO_2.

Meanwhile, an increase in the amount of adsorbed reactant does not continuously lead to an increase in the catalytic activity. Although the adsorbed amounts of GA and glucose increased linearly with increasing quantity of added AC in the adsorption tests (Figure 3.10), the TOR of Ru did not increase linearly, as shown in Figure 3.8. Hence, it can be concluded that the mixing effect of pristine AC is related to various other factors, in addition to the number of adsorption sites available for the reactants. Further studies are required to understand the factors that affect the effect of mixing pristine AC with a supported metal catalyst on biomass conversion.

Chapter 4. Conclusion and summary

Alginic acid was successfully converted to glycols such as ethylene glycol and 1,2-propanediol via hydrogenolysis over Ru-based activated carbon in a basic solution. In addition, various organic acids such as lactic acid, glycolic acid, and formic acid in the form of salts were produced. The type and concentration of the basic promoter strongly influenced the product distribution. Based on the hydrogenolysis of potential intermediates that can be produced from alginic acid under similar conditions, the direct conversion of alginic acid to glycols occurs via a retro-aldol reaction without intermediates such as sugar alcohols or organic acids under hydrogenolysis reaction conditions. The addition of Ni to activated carbon-supported Ru catalysts improved the yield of and selectivity to glycols obtained from alginic acid, and the optimal Ni/Ru molar ratio was 1. Furthermore, the positive effect of bimetallic Ru/Ni catalysts was verified by comparison with physically mixed Ru and Ni supported on activated carbon. The highest yield of glycols was 24.1% when $RuNi_1$/AC was used in 100 mM of NaOH solution. It is suggested that Ru-Ni bimetallic species formed via strong interaction

between Ru and Ni result in the enhanced hydrogenolysis of alginic acid to glycols.

A simple strategy of mixing a supported Ru catalyst with pristine AC was used to successfully enhance the utilization efficiency of Ru in the liquid-phase hydrogenation of gluconic acid (GA) into sorbitol. AC exhibited a mixing effect with the Ru catalysts supported on various oxides, regardless of the support type, indicating its effectiveness as an additive. In particular, Ru/SiO_2 exhibited the best catalytic activity when mixed with pristine AC. The turnover rate of Ru in the hydrogenation of GA over Ru/SiO_2 mixed with pristine AC increased significantly to 38.8 h^{-1}, compared to that of Ru/SiO_2 without pristine AC (12.8 h^{-1}). Various analyses suggested that pristine AC has adequate adsorption sites for the spilt-over hydrogen as well as the reactant.

In this thesis, the conversion of marine biomass-derived alginic acid and its intermediates was performed over ruthenium-based catalytic systems. The conversion of alginic acid into glycols is significant in that it further diversified alginic acid-derived products. In addition, the improvement of the efficiency of ruthenium in the hydrogenation through the addition of pristine activated carbon highlighted the potential for a physical mixing strategy in the liquid-phase. Thus, it is expected that this thesis will draw attention to

research on biorefinery of marine biomass and enable more efficient utilization of active metals.

Bibliography

[1] G. Erbach, L. Jensen, Fit for 55 package, European Parliamentary Research Service, 2022.

[2] Renewable Energy Market Update – Outlook for 2021 and 2022, IEA, 2021.

[3] F. Cherubini, G. Jungmeier, M. Wellisch, T. Willke, I. Skiadas, R. Van Ree, E. de Jong, Toward a common classification approach for biorefinery systems, Biofuels, Bioproducts and Biorefining 3(5) (2009) 534-546. https://doi.org/https://doi.org/10.1002/bbb.172.

[4] Biorefinery Market by Technology and Geography - Forecast and Analysis 2022-2026, technavio, 2022.

[5] J.A. Melero, J. Iglesias, A. Garcia, Biomass as renewable feedstock in standard refinery units. Feasibility, opportunities and challenges, Energy & environmental science 5(6) (2012) 7393-7420.

[6] K.A. Jung, S.-R. Lim, Y. Kim, J.M. Park, Potentials of macroalgae as feedstocks for biorefinery, Bioresource technology 135 (2013) 182-190.

[7] Renewable Biological Systems for Alternative Sustainable Energy Production, FAO (Food and Agriculture Organization of the United Nations), 2012b.

[8] V. Dhargalkar, N. Pereira, Seaweed: promising plant of the millennium, (2005).

[9] K.I. Draget, O. Smidsrød, G. Skjåk-Bræk, Alginates from algae, Polysaccharides and polyamides in the food industry: properties, production, and patents (2005) 1-30.

[10] R.L. Whistler, J. BeMiller, Alkaline Degradation of Alginates1, Journal of the American Chemical Society 82(2) (1960) 457-459.

[11] W. Jeon, C. Ban, G. Park, T.-K. Yu, J.-Y. Suh, H.C. Woo, D.H. Kim, Catalytic hydrothermal conversion of macroalgae-derived alginate: effect of pH on production of furfural and valuable organic acids under subcritical water conditions, Journal of Molecular Catalysis A: Chemical 399 (2015) 106-113.

[12] C. Ban, W. Jeon, G. Park, H.C. Woo, D.H. Kim, Hydrothermal Conversion of Alginate into Uronic Acids over a Sulfonated Glucose-Derived Carbon Catalyst, ChemCatChem 9(2) (2017) 329-337.

[13] G. Park, W. Jeon, C. Ban, H.C. Woo, D.H. Kim, Direct catalytic conversion of brown seaweed-derived alginic acid to furfural using 12-tungstophosphoric acid catalyst in tetrahydrofuran/water co-solvent, Energy Conversion and Management 118 (2016) 135-141.

[14] W. Jeon, C. Ban, G. Park, H.C. Woo, D.H. Kim, Hydrothermal conversion of alginic acid to furfural catalyzed by Cu (II) ion,

Catalysis Today 265 (2016) 154-162.

[15] W. Jeon, C. Ban, G. Park, H.C. Woo, D.H. Kim, Hydrothermal conversion of macroalgae-derived alginate to lactic acid catalyzed by metal oxides, Catalysis Science & Technology 6(4) (2016) 1146-1156.

[16] C. Ban, W. Jeon, H.C. Woo, D.H. Kim, Catalytic Hydrogenation of Macroalgae-Derived Alginic Acid into Sugar Alcohols, ChemSusChem 10(24) (2017) 4891-4898.

[17] C. Ban, S. Yang, H. Kim, D.H. Kim, Effect of Cu addition to carbon-supported Ru catalysts on hydrogenation of alginic acid into sugar alcohols, Applied Catalysis A: General 578 (2019) 98-104.

[18] C. Ban, S. Yang, H. Kim, D.H. Kim, Catalytic hydrogenation of alginic acid into sugar alcohols over ruthenium supported on nitrogen-doped mesoporous carbons, Catalysis Today 352 (2020) 66-72.

[19] V. Menon, M. Rao, Trends in bioconversion of lignocellulose: biofuels, platform chemicals & biorefinery concept, Progress in energy and combustion science 38(4) (2012) 522-550.

[20] A.J. Ragauskas, G.T. Beckham, M.J. Biddy, R. Chandra, F. Chen, M.F. Davis, B.H. Davison, R.A. Dixon, P. Gilna, M. Keller, Lignin valorization: improving lignin processing in the biorefinery, science 344(6185) (2014) 1246843.

[21] J. Sun, H. Liu, Selective hydrogenolysis of biomass-derived xylitol to ethylene glycol and propylene glycol on supported Ru catalysts, Green Chemistry 13(1) (2011) 135-142.

[22] I.M. Leo, M.L. Granados, J. Fierro, R. Mariscal, Selective conversion of sorbitol to glycols and stability of nickel–ruthenium supported on calcium hydroxide catalysts, Applied Catalysis B: Environmental 185 (2016) 141-149.

[23] M. Rivière, N. Perret, A. Cabiac, D. Delcroix, C. Pinel, M. Besson, Xylitol Hydrogenolysis over Ruthenium-Based Catalysts: Effect of Alkaline Promoters and Basic Oxide-Modified Catalysts, ChemCatChem 9(12) (2017) 2145-2159.

[24] Y. Amada, Y. Shinmi, S. Koso, T. Kubota, Y. Nakagawa, K. Tomishige, Reaction mechanism of the glycerol hydrogenolysis to 1, 3-propanediol over Ir–ReOx/SiO2 catalyst, Applied Catalysis B: Environmental 105(1-2) (2011) 117-127.

[25] A. Marinoiu, C. Cobzaru, E. Carcadea, C. Capris, V. Tanislav, M. Raceanu, Hydrogenolysis of glycerol to propylene glycol using heterogeneous catalysts in basic aqueous solutions, Reaction Kinetics, Mechanisms and Catalysis 110(1) (2013) 63-73.

[26] C. Montassier, J. Menezo, L. Hoang, C. Renaud, J. Barbier, Aqueous polyol conversions on ruthenium and on sulfur-modified ruthenium, Journal of Molecular Catalysis 70(1) (1991) 99-110.

[27] M. Banu, P. Venuvanalingam, R. Shanmugam, B. Viswanathan, S. Sivasanker, Sorbitol hydrogenolysis over Ni, Pt and Ru supported on NaY, Topics in Catalysis 55(11) (2012) 897-907.

[28] N. Ji, T. Zhang, M. Zheng, A. Wang, H. Wang, X. Wang, J.G. Chen, Direct catalytic conversion of cellulose into ethylene glycol using nickel-promoted tungsten carbide catalysts, Angewandte Chemie International Edition 47(44) (2008) 8510-8513.

[29] X. Chen, X. Wang, S. Yao, X. Mu, Hydrogenolysis of biomass-derived sorbitol to glycols and glycerol over Ni-MgO catalysts, Catalysis Communications 39 (2013) 86-89.

[30] A.G. Sergeev, J.F. Hartwig, Selective, nickel-catalyzed hydrogenolysis of aryl ethers, Science 332(6028) (2011) 439-443.

[31] L.S. Ribeiro, J.J. Delgado, J.J. Órfão, M.F.R. Pereira, Carbon supported Ru-Ni bimetallic catalysts for the enhanced one-pot conversion of cellulose to sorbitol, Applied Catalysis B: Environmental 217 (2017) 265-274.

[32] L. Yang, J. Su, S. Carl, J.G. Lynam, X. Yang, H. Lin, Catalytic conversion of hemicellulosic biomass to lactic acid in pH neutral aqueous phase media, Applied catalysis B: environmental 162 (2015) 149-157.

[33] T. Komanoya, H. Kobayashi, K. Hara, W.-J. Chun, A. Fukuoka, Catalysis and characterization of carbon-supported ruthenium for

cellulose hydrolysis, Applied Catalysis A: General 407(1-2) (2011) 188-194.

[34] A. Calafat, J. Laine, A. López-Agudo, J. Palacios, Effect of surface oxidation of the support on the thiophene hydrodesulfurization activity of Mo, Ni, and NiMo catalysts supported on activated carbon, Journal of Catalysis 162(1) (1996) 20-30.

[35] C. Crisafulli, S. Scirè, R. Maggiore, S. Minicò, S. Galvagno, CO2 reforming of methane over Ni–Ru and Ni–Pd bimetallic catalysts, Catalysis Letters 59(1) (1999) 21-26.

[36] M. Cerro-Alarcón, A. Guerrero-Ruíz, I. Rodríguez-Ramos, Stereoselective hydrogenation of Paracetamol to trans-4-acetamidocyclohexanol on carbon-supported Ru□ M (M= Co, Ni) bimetallic catalysts, Catalysis today 93 (2004) 395-403.

[37] F. Liu, J.Y. Lee, W.J. Zhou, Segmented Pt/Ru, Pt/Ni, and Pt/RuNi nanorods as model bifunctional catalysts for methanol oxidation, Small 2(1) (2006) 121-128.

[38] H. Shimizu, K. Christmann, G. Ertl, Model studies on bimetallic Cu/Ru catalysts: II. Adsorption of hydrogen, Journal of Catalysis 61(2) (1980) 412-429.

[39] K. Matsushima, H. Minoshima, H. Kawanami, Y. Ikushima, M. Nishizawa, A. Kawamukai, K. Hara, Decomposition reaction of alginic acid using subcritical and supercritical water, Industrial &

engineering chemistry research 44(25) (2005) 9626-9630.

[40] E.P. Maris, R.J. Davis, Hydrogenolysis of glycerol over carbon-supported Ru and Pt catalysts, Journal of Catalysis 249(2) (2007) 328-337.

[41] M. Liu, H. Wang, J. Han, Y. Niu, Enhanced hydrogenolysis conversion of cellulose to C2–C3 polyols via alkaline pretreatment, Carbohydrate polymers 89(2) (2012) 607-612.

[42] P. Lazaridis, S. Karakoulia, C. Teodorescu, N. Apostol, D. Macovei, A. Panteli, A. Delimitis, S. Coman, V. Parvulescu, K. Triantafyllidis, High hexitols selectivity in cellulose hydrolytic hydrogenation over platinum (Pt) vs. ruthenium (Ru) catalysts supported on micro/mesoporous carbon, Applied Catalysis B: Environmental 214 (2017) 1-14.

[43] P.J. Hausoul, L. Negahdar, K. Schute, R. Palkovits, Unravelling the Ru-Catalyzed Hydrogenolysis of Biomass-Based Polyols under Neutral and Acidic Conditions, ChemSusChem 8(19) (2015) 3323-3330.

[44] K. Niemelä, E. Sjöström, Alkaline degradation of alginates to carboxylic acids, Carbohydrate research 144(2) (1985) 241-249.

[45] S. Valizadeh, S.S. Lam, C.H. Ko, S.H. Lee, A. Farooq, Y.J. Yu, J.-K. Jeon, S.-C. Jung, G.H. Rhee, Y.-K. Park, Biohydrogen production from catalytic conversion of food waste via steam and air

gasification using eggshell-and homo-type Ni/Al2O3 catalysts, Bioresource technology 320 (2021) 124313.

[46] J.-Y. Kim, H.W. Lee, S.M. Lee, J. Jae, Y.-K. Park, Overview of the recent advances in lignocellulose liquefaction for producing biofuels, bio-based materials and chemicals, Bioresource technology 279 (2019) 373-384.

[47] M.W. Seo, S.H. Lee, H. Nam, D. Lee, D. Tokmurzin, S. Wang, Y.-K. Park, Recent advances of thermochemical conversion processes for biorefinery, Bioresource Technology 343 (2022) 126109.

[48] H.W. Ryu, Y.F. Tsang, H.W. Lee, J. Jae, S.-C. Jung, S.S. Lam, E.D. Park, Y.-K. Park, Catalytic co-pyrolysis of cellulose and linear low-density polyethylene over MgO-impregnated catalysts with different acid-base properties, Chemical Engineering Journal 373 (2019) 375-381.

[49] S. Oh, J. Lee, S.S. Lam, E.E. Kwon, J.-M. Ha, D.C. Tsang, Y.S. Ok, W.-H. Chen, Y.-K. Park, Fast hydropyrolysis of biomass Conversion: A comparative review, Bioresource technology 342 (2021) 126067.

[50] P. Gallezot, N. Nicolaus, G. Fleche, P. Fuertes, A. Perrard, Glucose hydrogenation on ruthenium catalysts in a trickle-bed reactor, Journal of Catalysis 180(1) (1998) 51-55.

[51] P.P. Upare, J.-M. Lee, D.W. Hwang, S.B. Halligudi, Y.K. Hwang, J.-S. Chang, Selective hydrogenation of levulinic acid to γ-valerolactone over carbon-supported noble metal catalysts, Journal of industrial and engineering chemistry 17(2) (2011) 287-292.

[52] H.-T. Vu, F.M. Harth, M. Goepel, N. Linares, J. García–Martínez, R. Gläser, Enhanced activity of a bifunctional Pt/zeolite Y catalyst with an intracrystalline hierarchical pore system in the aqueous-phase hydrogenation of levulinic acid, Chemical Engineering Journal 430 (2022) 132763.

[53] L. Wang, L. Wang, X. Meng, F.S. Xiao, New strategies for the preparation of sinter-resistant metal-nanoparticle-based catalysts, Advanced Materials 31(50) (2019) 1901905.

[54] Y. Shao, S. Ba, K. Sun, G. Gao, M. Fan, J. Wang, H. Fan, L. Zhang, X. Hu, Selective production of γ-valerolactone or 1, 4-pentanediol from levulinic acid/esters over Co-based catalyst: Importance of the synergy of hydrogenation sites and acidic sites, Chemical Engineering Journal 429 (2022) 132433.

[55] H.J. Bixler, H. Porse, A decade of change in the seaweed hydrocolloids industry, Journal of applied Phycology 23(3) (2011) 321-335.

[56] D.J. McHugh, A guide to the seaweed industry FAO Fisheries Technical Paper 441, Food and Agriculture Organization of the

United Nations, Rome 110 (2003).

[57] X. Guo, Y. Wang, Y. Qin, P. Shen, Q. Peng, Structures, properties and application of alginic acid: A review, International Journal of Biological Macromolecules 162 (2020) 618-628.

[58] R. Prins, Hydrogen spillover. Facts and fiction, Chemical reviews 112(5) (2012) 2714-2738.

[59] M. Xiong, Z. Gao, Y. Qin, Spillover in heterogeneous catalysis: new insights and opportunities, ACS Catalysis 11(5) (2021) 3159-3172.

[60] W.C. Conner Jr, J.L. Falconer, Spillover in heterogeneous catalysis, Chemical reviews 95(3) (1995) 759-788.

[61] S. Srinivas, P.K. Rao, Direct observation of hydrogen spillover on carbon-supported platinum and its influence on the hydrogenation of benzene, Journal of Catalysis 148(2) (1994) 470-477.

[62] S. Lee, K. Lee, J. Im, H. Kim, M. Choi, Revisiting hydrogen spillover in Pt/LTA: Effects of physical diluents having different acid site distributions, Journal of Catalysis 325 (2015) 26-34.

[63] A.D. Lueking, R.T. Yang, Hydrogen spillover to enhance hydrogen storage—study of the effect of carbon physicochemical properties, Applied Catalysis A: General 265(2) (2004) 259-268.

[64] L.R. Merte, G. Peng, R. Bechstein, F. Rieboldt, C.A. Farberow, L.C. Grabow, W. Kudernatsch, S. Wendt, E. Lægsgaard, M. Mavrikakis,

Water-mediated proton hopping on an iron oxide surface, Science 336(6083) (2012) 889-893.

[65] J. Shangguan, Y.-H.C. Chin, Kinetic significance of proton–electron transfer during condensed phase reduction of carbonyls on transition metal clusters, ACS Catalysis 9(3) (2019) 1763-1778.

[66] D.D. Hibbitts, B.T. Loveless, M. Neurock, E. Iglesia, Mechanistic role of water on the rate and selectivity of Fischer–Tropsch synthesis on ruthenium catalysts, Angewandte Chemie International Edition 52(47) (2013) 12273-12278.

[67] J. Zhao, B. Li, K. Onda, M. Feng, H. Petek, Solvated electrons on metal oxide surfaces, Chemical reviews 106(10) (2006) 4402-4427.

[68] H. Shiraishi, Y. Katsumura, D. Hiroishi, K. Ishigure, M. Washio, Pulse-radiolysis study on the yield of hydrated electron at elevated temperatures, The Journal of Physical Chemistry 92(10) (1988) 3011-3017.

[69] H. Kim, S. Yang, Y.H. Lim, J. Lee, J.-M. Ha, D.H. Kim, Enhancement in the metal efficiency of Ru/TiO2 catalyst for guaiacol hydrogenation via hydrogen spillover in the liquid phase, Journal of Catalysis 410 (2022) 93-102.

[70] Q. Zhou, Z. Zhao, Z. Yao, Z. Wei, S. Huang, F. Shao, A. Li, J. Wang, Engineering the geometric and electronic structure of Ru via

Ru–TiO 2 interaction for enhanced selective hydrogenation, Catalysis Science & Technology 12(3) (2022) 1005-1016.

[71] Y. Zhang, X. Su, L. Li, H. Qi, C. Yang, W. Liu, X. Pan, X. Liu, X. Yang, Y. Huang, Ru/TiO2 catalysts with size-dependent metal/support interaction for tunable reactivity in Fischer–Tropsch synthesis, ACS Catalysis 10(21) (2020) 12967-12975.

[72] V. Mazzieri, F. Coloma-Pascual, A. Arcoya, P. L'Argentière, N. Fıgoli, XPS, FTIR and TPR characterization of Ru/Al2O3 catalysts, Applied Surface Science 210(3-4) (2003) 222-230.

[73] X. Liao, K. Li, X. Xiang, S.-G. Wang, X. She, Y. Zhu, Y. Li, Mediatory role of K, Cu and Mo over Ru/SiO2 catalysts for glycerol hydrogenolysis, Journal of Industrial and Engineering Chemistry 18(2) (2012) 818-821.

[74] L. Fabre, G. Flèche, P. Fuertes, P. Gallezot, A. Perrard, Hydrogenation of gluconolactones in equilibrium with gluconic acid on ruthenium catalyst, Catalysis letters 68(1) (2000) 41-44.

[75] Z. Zhang, P. Gibson, S.B. Clark, G. Tian, P.L. Zanonato, L. Rao, Lactonization and protonation of gluconic acid: a thermodynamic and kinetic study by potentiometry, NMR and ESI-MS, Journal of Solution Chemistry 36(10) (2007) 1187-1200.

[76] J. Da-Silva, A. Cobo, The role of the titania and silica supports in Ru-Fe catalysts to partial hydrogenation of benzene, Applied

Catalysis A: General 252(1) (2003) 9-16.

[77] S. Pevzner, I. Pri-Bar, I. Lutzky, E. Ben-Yehuda, E. Ruse, O. Regev, Carbon allotropes accelerate hydrogenation via spillover mechanism, The Journal of Physical Chemistry C 118(46) (2014) 27164-27169.

[78] I.C. Gerber, P. Serp, A theory/experience description of support effects in carbon-supported catalysts, Chemical Reviews 120(2) (2019) 1250-1349.

[79] E. Crezee, B.W. Hoffer, R.J. Berger, M. Makkee, F. Kapteijn, J.A. Moulijn, Three-phase hydrogenation of D-glucose over a carbon supported ruthenium catalyst—mass transfer and kinetics, Applied Catalysis A: General 251(1) (2003) 1-17.

[80] J. Wisnlak, R. Simon, Hydrogenation of glucose, fructose, and their mixtures, Industrial & Engineering Chemistry Product Research and Development 18(1) (1979) 50-57.

[81] B. Lin, R. Wang, X. Yu, J. Lin, F. Xie, K. Wei, Physicochemical characterization and H2-TPD study of alumina supported ruthenium catalysts, Catalysis letters 124(3) (2008) 178-184.

[82] B. Lin, R. Wang, J. Lin, J. Ni, K. Wei, Effect of chlorine on the chemisorptive properties and ammonia synthesis activity of alumina-supported Ru catalysts, Catalysis letters 141(10) (2011) 1557-1568.

[83] A. Guntida, K. Suriye, J. Panpranot, P. Praserthdam,

Comparative study of lewis acid transformation on non-reducible and reducible oxides under hydrogen atmosphere by in situ DRIFTS of adsorbed NH3, Topics in Catalysis 61(15) (2018) 1641-1652.

[84] S. Suganuma, K. Nakajima, M. Kitano, D. Yamaguchi, H. Kato, S. Hayashi, M. Hara, Hydrolysis of cellulose by amorphous carbon bearing SO3H, COOH, and OH groups, Journal of the American Chemical Society 130(38) (2008) 12787-12793.

[85] M. Kitano, D. Yamaguchi, S. Suganuma, K. Nakajima, H. Kato, S. Hayashi, M. Hara, Adsorption-enhanced hydrolysis of β-1, 4-glucan on graphene-based amorphous carbon bearing SO3H, COOH, and OH groups, Langmuir 25(9) (2009) 5068-5075.

국 문 초 록

지구 평균온도 상승폭을 1.5 ℃ 이내로 제한하기 위한 국가적 차원에서의 탄소중립은 더 이상 선택이 아닌 의무적인 국가 정책이 되었다. 이러한 글로벌 흐름에 발맞추어 우리나라 또한 2050 탄소중립 달성을 위해 경제•사회적 대전환을 법제화한 탄소중립기본법을 본격 시행할 예정이다. 이 과정에서 신재생에너지의 활용성을 극대화하는 것이 최대의 과제라 할 수 있다. 신재생에너지는 재생 가능한 자원, 즉 햇빛(태양), 바람(풍력), 조수(조력), 생물 자원(바이오매스), 지열과 같이 시간이 지남에 따라 자연적으로 보충되는 자원으로부터 수집되는 에너지를 뜻한다. 신재생에너지 분야 중에서도 전력 생산을 위한 태양열, 풍력 에너지 등에 대한 연구가 활발히 진행되고 있다. 반면, 다양한 화학 제품을 생산하기 위한 원유 기반 공정을 대체할 수 있는 탄소 자원의 신재생에너지는 바이오매스가 유일하다.

바이오리파이너리는 연료와 플라스틱, 섬유 등의 화학 제품을 기존원유 자원이 아닌 바이오매스 자원으로 대체하여 생산하는 공정을 뜻한다. 바이오리파이너리의 특징은 (1) 플랫폼, (2) 제품, (3) 원료, (4) 과정의 네 가지로 분류할 수 있으며 특징 별로 다양한 하위 집단이 구성된다. 해당 분류 체계 하에서 바이오리파이너리의 설계를 위해 고려해야 할 이슈로 바이오매스 원료 공급망, 온실 가스 배출량, 가격 경쟁력 등이 있다. 상기의 이슈를 고려했을 때, 해양 바이오매스는 기존 육상 바이오매스와 달리 비식용 자원이며 생장 속도가 빠르고 난분해성 리그닌 성분을 함유하지 않는 등의 장점을 가진다. 특히, 해양 바이오매스 중 갈조류의 주요 구성 성분인

알긴산 고분자는 카르복실기를 포함하고 있어, 육상 바이오매스의 대표적 플랫폼인 리그닌 혹은 셀룰로오스에서 얻을 수 없는 다양한 제품을 생산할 수 있다. 더 나아가, 알긴산의 열화학적 전환 과정에서 사용되는 불균일계 촉매계에 따라 제품군이 보다 다양해질 수 있다.

본 연구에서는 해양 바이오매스 유래 알긴산과 그 중간체를 반응물로 하는 열수 반응을 루테늄계 촉매 시스템 하에서 수행하였다. 이에 따라, 알긴산으로부터 수득되는 화합물 포트폴리오를 다양화하기 위한 촉진제 및 루테늄의 효율을 증가시키기 위한 촉매 시스템에 대한 전략을 중점적으로 모색하였다.

우선, 루테늄 기반 활성탄 촉매 하에서 반응 용액의 pH를 높이는 염기를 촉진제로써 첨가하여 탄소 수 3개 이하의 알코올류를 획득하고자 하였다. 이에 따라, 루테늄 및 루테늄-니켈 이종 금속이 담지된 활성탄 촉매 하에서 알긴산의 수소첨가분해반응을 높은 pH에서 수행하였다. pH를 높이기 위해 다양한 염기(수산화나트륨, 탄산칼슘, 수산화칼슘 및 수산화마그네슘)를 사용하였으며, 그 중에서 수산화나트륨은 가장 높은 탄소 효율과 함께 에틸렌 글리콜 및 프로필렌글리콜(1,2-프로판디올)과 같은 글리콜에 대한 가장 높은 수율을 제공하였다. 소르비톨, 만니톨, 자일리톨, 락트산 및 글리콜산과 같은 잠재적 중간체의 수소첨가분해반응은 반응 중간체로서 당 알코올 또는 유기산 없이 알긴산에서 글리콜로의 직접적인 전환됨을 입증하였다. 또한 니켈/루테늄 몰 비율에 따라 제조된 루테늄-니켈 이종 금속 촉매를 사용하여 글리콜의 수율과 선택도를 증진시켰다. 결과적으로, 니켈/루테늄 몰 비율이 1일 때, 글리콜을 24.1%의 최대 수율로 전환시켰으며, 루테

늄과 니켈 사이에 형성되는 강한 전자적 상호작용과 연관됨을 입증하였다.

또한, 기존에 보고된 불균일계 촉매의 효율을 개선하기 위한 연구는 고도로 지속 가능한 바이오리파이너리의 생산 효율성을 향상시키는 데에 있어 필수 전략이다. 알긴산은 루테늄 기반의 불균일계 촉매 하에서 가수분해 및 수소화반응을 통해 소르비톨과 만니톨과 같은 고부가가치의 6탄당알코올로 전환된다. 상기의 촉매 시스템에서 루테늄의 효율을 향상시키기 위해 액상 수소화반응에서의 입자 간 수소 스필오버 기작에 대한 활용 가능성을 검증하고자 하였다. 이에 따라, 순수 담체(활성탄, 실리카, 타이타니아, 알루미나)와 물리 혼합된 루테늄 기반 촉매 하에서 알긴산 가수분해 및 수소화반응의 중간체인 글루콘산에서 소르비톨로의 수소화반응을 진행하였다. 활성탄과 물리 혼합한 모든 루테늄 촉매에서 루테늄의 전환율이 증가하였으며, 특히 Ru/SiO_2 촉매의 경우 12.8 h^{-1}에서 38.8 h^{-1}로 가장 큰 폭으로 증가하였다. 다양한 촉매 특성 분석에 따르면, 첨가된 활성탄은 루테늄으로부터 스필오버된 활성 수소를 더 많이 흡수할 수 있고 다른 담체에 비해 반응물에 대한 우수한 흡착 능력으로 인해 추가적인 촉매 활성 부위를 제공한다. 해당 연구 결과, 액상에서의 입자 간 수소 스필오버 활용을 위해 활성탄을 루테늄 기반 촉매와 함께 물리 혼합하는 비교적 간단한 전략을 통해 루테늄의 전환율을 크게 향상시켰다.

본 연구에서는 루테늄 기반 촉매를 사용하여 해양 바이오매스 유래 알긴산 전환을 수행하였다. 알긴산으로부터 글리콜로의 전환은 알긴산 유래 화합물을 보다 다양화시켰다는 점에서 의의가 있다. 또한, 액상에서의 수소 스필오버 기작을 활용한 활성탄의 첨가 효과를 통해 수소화반응에서 루테

늄의 효율을 큰 폭으로 향상시킴에 따라 금속 촉매와 순수 담체의 물리 혼합 전략에 대한 잠재성을 부각시켰다는 점 또한 의의가 있다. 본 연구를 통해 해양 바이오매스에 대한 바이오리파이너리 연구 관심을 환기시키고 활성 금속에 대한 보다 효율적인 활용이 가능해질 것이라 기대된다.

주요어: 알긴산, 글루콘산, 수소첨가분해반응, 수소화반응, 글리콜, 소르비톨, 루테늄 촉매, 활성탄